J Physiol 592.14 (2014) pp 3089–3111

The Journal of Physiology

$P2Y_1$ receptor-mediated potentiation of inspiratory motor output in neonatal rat *in vitro*

T. S. Alvares, A. L. Revill, A. G. Huxtable, C. D. Lorenz and G. D. Funk

Department of Physiology, Centre for Neuroscience, Women and Children's Health Research Institute (WCHRI), Faculty of Medicine and Dentistry, University of Alberta, Edmonton, Alberta, Canada

Key points

- The role of metabotropic purinergic receptors (P2YRs) in modulating motor output from the CNS is virtually unknown, despite the fact that many motoneurons, including respiratory motoneurons, express P2YRs.
- Using rhythmically active brainstem–spinal cord and medullary slice preparations, we demonstrate that compared to the 4th cervical spinal nerve (C4) inspiratory output controlling the diaphragm, P2YR activation is >10 times more efficacious at potentiating the hypoglossal nerve (XII) inspiratory output controlling airway muscles.
- P2YR potentiation of inspiratory output appears largely mediated by $P2Y_1R$.
- Whole-cell recordings from XII motoneurons (MNs) suggest that the $P2Y_1R$-mediated potentiation of inspiratory synaptic inputs, glutamate currents, and persistent inward currents, results in part from potentiation of a transient receptor potential cation channel, subfamily M, member 4 (TRPM4)-mediated, calcium-activated, non-specific cation current, I_{CAN}.
- The low sensitivity of phrenic output to P2YR activation questions its physiological significance in modulating diaphragm activity. However, the greater sensitivity of XII MNs, combined with observations that ATP is often co-released with noradrenaline and that noradrenergic neuron activity decreases in sleep, makes it tempting to speculate that loss of purinergic modulation contributes to state-dependent reductions in XII MN excitability.

Abstract PreBötzinger complex inspiratory rhythm-generating networks are excited by metabotropic purinergic receptor subtype 1 ($P2Y_1R$) activation. Despite this, and the fact that inspiratory MNs express $P2Y_1Rs$, the role of $P2Y_1Rs$ in modulating motor output is not known for any MN pool. We used rhythmically active brainstem–spinal cord and medullary slice preparations from neonatal rats to investigate the effects of $P2Y_1R$ signalling on inspiratory output of phrenic and XII MNs that innervate diaphragm and airway muscles, respectively. MRS2365 ($P2Y_1R$ agonist, 0.1 mM) potentiated XII inspiratory burst amplitude by 60 ± 9%; 10-fold higher concentrations potentiated C4 burst amplitude by 25 ± 7%. In whole-cell voltage-clamped XII MNs, MRS2365 evoked small inward currents and potentiated spontaneous EPSCs and inspiratory synaptic currents, but these effects were absent in TTX at resting membrane potential. Voltage ramps revealed a persistent inward current (PIC) that was attenuated by: flufenamic acid (FFA), a blocker of the Ca^{2+}-dependent non-selective cation current I_{CAN}; high intracellular concentrations of BAPTA, which buffers Ca^{2+} increases necessary for activation of I_{CAN}; and 9-phenanthrol, a selective blocker of TRPM4 channels (candidate for I_{CAN}). Real-time PCR analysis of mRNA extracted from XII punches and laser-microdissected XII MNs revealed the transcript for TRPM4. MRS2365 potentiated the PIC and this potentiation was blocked by FFA,

T. S. Alvares and A. L. Revill are co-first authors and contributed equally to this work.

DOI: 10.1113/jphysiol.2013.268136

which also blocked the MRS2365 potentiation of glutamate currents. These data suggest that XII MNs are more sensitive to $P2Y_1R$ modulation than phrenic MNs and that the $P2Y_1R$ potentiation of inspiratory output occurs in part via potentiation of TRPM4-mediated I_{CAN}, which amplifies inspiratory inputs.

(Received 25 December 2013; accepted after revision 14 May 2014; first published online 30 May 2014)
Corresponding author G. D. Funk: 3-020G Katz Group Centre, Department of Physiology, University of Alberta, Edmonton, Alberta, Canada, T6G 2E1. Email: gf@ualberta.ca

Abbreviations aCSF, artificial cerebrospinal fluid; BSSC, brainstem–spinal cord; C4, 4th cervical spinal nerve; ChAT, choline acetyl transferase; FFA, flufenamic acid; I_{CAN}, calcium-dependent, non-selective cation current; I_{NaP}, persistent sodium current; IRDIC, infrared differential interference contrast; LCM, laser-capture microdissection; mEPSC, miniature excitatory postsynaptic current; mGluR, metabotropic glutamate receptor; MN, motoneuron; NK1R, neurokinin 1 receptor for the neuromodulator substance P; P2, purinergic receptor; P2X, ionotropic P2 receptor; P2Y, metabotropic P2 receptor; PIC, persistent inward current; preBötC, preBötzinger complex; PSC, postsynaptic current; SD, Sprague–Dawley; TRPM4 and TRPM5, transient receptor potential cation channel, subfamily M, member 4 and 5; UTP, uridine triphosphate; XII, hypoglossal nerve.

Introduction

ATP acts as a transmitter in the central nervous system (CNS) by binding to two types of purinergic (P2) receptors (Rs). P2XRs are ionotropic, cation-selective, ligand-gated ion channels that comprise seven subtypes ($P2X_{1–7}$) (North, 2002). P2YRs are metabotropic, G-protein-coupled receptors that signal through slower, second messenger cascades and comprise at least eight subtypes ($P2Y_{1,2,4,6,11–14}$) (Illes & Alexandre Ribeiro, 2004; Illes & Ribeiro, 2004). P2X and P2Y receptors are distributed throughout the brain, including brainstem regions involved in cardiorespiratory control (Kanjhan 1999; Thomas *et al.* 2001; Yao *et al.* 2001; Fong *et al.* 2002; Gourine *et al.* 2003; Lorier *et al.* 2004, 2007; Mulkey *et al.* 2006; Burnstock, 2007; Funk *et al.* 2008). ATP is now widely recognized not only as a neurotransmitter in multiple brain regions (Burnstock, 2007), but also as a gliotransmitter released by astrocytes that influences neurons and glia alike (Abbracchio *et al.* 2009).

A potential role for ATP in motor control was first demonstrated in *Xenopus* embryos where an interaction between the excitatory actions of ATP via a P2YR-like mechanism and the inhibitory actions of adenosine via P1Rs participate in controlling episodic motor patterns (Dale & Gilday, 1996). A role for ATP signalling in motor control within the mammalian CNS is supported by the sensitivity of brainstem inspiratory rhythm-generating networks to ATP (Lorier *et al.* 2007, 2008; Huxtable *et al.* 2010; Zwicker *et al.* 2011), and the ubiquitous expression of P2Rs on MNs (Collo *et al.* 1996; Funk *et al.* 1997; Miles *et al.* 2002; Kobayashi *et al.* 2006). Purinergic modulation of MN excitability in the mammalian CNS was first demonstrated in the respiratory network. In XII MNs that innervate muscles of the tongue important for maintaining airway patency (Funk *et al.* 1997), and to a lesser extent phrenic MNs that innervate the main inspiratory pump muscle, the diaphragm, ATP is excitatory and potentiates inspiratory output (Funk *et al.* 1997; Miles *et al.* 2002). ATP excitation is probably mediated in part by a $P2X_2R$ mechanism, but a presynaptic $P2X_7R$ mechanism may contribute at XII MNs (Ireland *et al.* 2004). Whether P2YR signalling modulates MN excitability is not known, but preBötzinger complex (preBötC) inspiratory rhythm-generating networks are very sensitive to $P2Y_1R$-mediated excitation (Lorier *et al.* 2007). XII MNs also show immunolabelling for $P2Y_1Rs$ (Fong *et al.* 2002). Thus, the objectives of this study were to determine, using rhythmically active brainstem–spinal cord and medullary slice preparations from neonatal rats, whether inspiratory motor output of phrenic and XII MNs is sensitive to $P2Y_1R$ modulation and to define underlying mechanisms. We specifically tested the hypothesis that potentiation of I_{CAN} is a target through which $P2Y_1Rs$ modulate inspiratory MN output based on the observations that: (i) $P2Y_1Rs$ activate phospholipase C (Simon *et al.* 1995; von Kugelgen & Wetter, 2000; Sak & Illes, 2005) which, through phosphatidylinositol 4,5-bisphosphate (PIP_2), *myo*-inositol 1,4,5-trisphosphate (IP_3) and possibly also increases in intracellular Ca^{2+}, enhances the TRPM4/5 conductance (Crowder *et al.* 2007; Pace *et al.* 2007; Mironov, 2008; Guinamard *et al.* 2011; Mironov & Skorova, 2011; Mironov, 2013) believed to underlie I_{CAN} (Launay *et al.* 2002; Hofmann *et al.* 2003; Nilius *et al.* 2005; Ullrich *et al.* 2005); (ii) juvenile XII MNs express TRPM4 (Funk *et al.* 2011); and (iii) I_{CAN} amplifies inspiratory currents in preBötC inspiratory neurons (Pace *et al.* 2007), which also express TRPM4/5 (Crowder *et al.* 2007). We focused on phrenic and XII MNs because *in vitro* data suggest that phrenic inspiratory activity (Miles *et al.* 2002) is less sensitive to ATP modulation than XII output (Funk *et al.* 1997). Understanding the differential modulation of MNs controlling pump and airway muscles by ATP is important because a mismatch in

the inspiratory output of these two pools could contribute to the pathology of sleep-related disorders of breathing (Hudgel & Harasick, 1990). ATP is co-released with noradrenaline (norepinephrine) at some central synapses (Poelchen *et al.* 2001). Thus, state-dependent reductions in noradrenaline release that are implicated in airway muscle atonia in sleep (Chan *et al.* 2006) may include reductions in ATP.

Methods

Ethical approval

All experimental procedures were approved by the University of Alberta Faculty of Medicine Animal Welfare Committee and performed in accordance with their guidelines for the care, handling and treatment of experimental animals.

Animals

Experiments were performed using neonatal rats ranging in age from postnatal day 0–4 (P0–P4). Both Wistar and Sprague–Dawley (SD) rat pups were used for the nerve recording experiments in which the effects of P2YR activation on C4 and XII inspiratory motor output were examined using the brainstem–spinal cord and rhythmic medullary slice preparations described below. No differences were detected between strains so these data were pooled. All whole-cell recording experiments were performed on SD rats.

Preparations

Brainstem–spinal cord (BSSC) preparations were isolated using methods described previously (Suzue, 1984; Smith & Feldman, 1987; Miles *et al.* 2002). Briefly, animals were anaesthetized through inhalation of isoflurane and decerebrated. The BSSC was isolated in cold (5–10°C), artificial cerebrospinal fluid (aCSF) containing (in mM): 120 NaCl, 3 KCl, 1 $CaCl_2$, 2 $MgSO_4$, 26 $NaHCO_3$, 1.25 NaH_2PO_4, and 20 D-glucose, equilibrated with 95% O_2–5% CO_2. BSSC preparations were transected at the pontomedullary border and between cervical segments 7 and 8 (C7 and C8), pinned with the ventral surface up on Sylgard resin in a recording chamber (volume, 10 ml) and perfused with aCSF that was recirculated at a flow rate of 12 ml min^{-1}. Unless stated otherwise, all experiments (BSSC and slices) were conducted at a temperature of 25–27°C.

Rhythmic slice preparations were produced as described elsewhere (Smith *et al.* 1991; Ruangkittisakul *et al.* 2006; Lorier *et al.* 2007). Briefly, the BSSC was pinned to a wax chuck and serial 100–200 μm sections were cut in the rostral to caudal direction using a vibratome (Leica VT-1000S, Concord, ON, Canada). Sections were transilluminated to identify anatomical landmarks, and referenced against the neonatal rat brainstem atlas (Ruangkittisakul *et al.* 2006). A single 700 μm slice was cut after the compact division of nucleus ambiguus was no longer evident and the rostral margin of the inferior olive first appeared in the thin sections (−0.35 mm caudal to the caudal aspect of the facial nucleus) (Smith *et al.* 1991; Ruangkittisakul *et al.* 2006; Lorier *et al.* 2007). The caudal boundary of the 700 μm rhythmic slice was just caudal to the obex. Slices contained the preBötC, rostral ventral respiratory group, most of the XII motor nuclei and the rostral XII nerve rootlets. For nerve recording experiments, slices were pinned with the caudal surface up in a recording chamber (volume, 10 ml) and perfused with aCSF that was recirculated at a flow rate of 12 ml min^{-1}.

For whole-cell recording experiments, rhythmic slices were used to examine mechanisms by which $P2Y_1R$ modulation affected endogenous glutamatergic synaptic input and inspiratory synaptic drive. These slices were placed caudal surface up in the recording chamber of an upright microscope (Zeiss Axioskop 2 FS Plus, Toronto, ON, Canada) equipped with infrared differential interference contrast optics (IRDIC) and epifluorescence. Slices were held in place with a platinum harp and perfused continuously at a flow rate of 1–2 ml min^{-1}. The concentration of K^+ in the aCSF ($[K^+]_o$) was raised from 3 to 9 mM at least 30 min prior to the start of data collection. Elevated $[K^+]_o$ is not a necessary condition for rhythm generation. Medullary slices from neonatal rats that are 700 μm thick generate stable respiratory rhythm in 3 mM $[K^+]_o$ for 2 h on average, after which rhythm gradually slows over the next 2 h and then ceases (Ruangkittisakul *et al.* 2006). However, the protocols with rhythmic slices involved multiple interventions, and therefore required slices that produced stable inspiratory-related rhythm for extended periods (i.e. >5 h). Therefore, the $[K^+]_o$ was raised from 3 to 9 mM. Elevated $[K^+]_o$ is proposed to compensate for the loss of excitatory/modulatory input (for additional discussions see: Smith *et al.* 1991; Funk *et al.* 1993; Ruangkittisakul *et al.* 2006).

Non-rhythmic slices were used to explore the mechanisms by which $P2Y_1Rs$ affected XII MN properties as this increased experimental yield; i.e. only one rhythmic slice can be produced per neonatal rat whereas 2–3 non-rhythmic slices containing the XII nucleus can be produced per rat. Non-rhythmic slices were produced using procedures similar to those described previously (Adachi *et al.* 2010). The BSSC was pinned to a wax chuck and serial 100–200 μm sections were cut until the rostral margin of the XII nucleus was visible in transilluminated sections. Two to three slices (300 μm) containing the XII nucleus were then collected and transferred to a holding chamber containing standard aCSF

at room temperature for at least 1 h prior to recording. Unless stated otherwise, experiments on non-rhythmic slices were performed in aCSF containing 3 mM K^+.

Nerve recordings

Inspiratory-related activity was recorded from severed ends of C4 (in BSSC preparations), or XII (in rhythmic slice preparations) nerve roots using glass suction electrodes (80–120 μm i.d.). Signals were amplified, band-pass filtered (300 Hz to 1 kHz) (A-M Systems, Carlsborg, WA, USA), full-wave rectified, integrated using a leaky integrator (τ = 50 ms, Moving Averager, CWE Inc., Ardmore, PA, USA), and displayed on a computer monitor using AxoScope 9.2 software (pCLAMP Suite, Molecular Devices, Sunnyvale, CA, USA). Data were saved to computer using a Digidata 1322 A/D board (Molecular Devices) and AxoScope software for off-line analysis.

MN identification

Neurons were identified as XII MNs based on their location within the XII nucleus and characteristic morphology, both of which are easily established under visualization with IRDIC microscopy (Funk *et al.* 1993; Stuart *et al.* 1993; Adachi *et al.* 2005, 2010). The XII nucleus is relatively homogeneous; less than 5% are interneurons (Viana *et al.* 1990). Morphological criteria included a large cell soma that was >15 μm along the shortest axis, 20–30 μm in the longest axis (Núñez-Abades *et al.* 1994; Núñez-Abades & Cameron, 1995). MNs were included in the analysis if they had a resting membrane potential of –40 mV or more hyperpolarized in aCSF at 9 mM K^+, or −50 mV or more hyperpolarized in aCSF at 3 mM K^+ and Cs^+-based intracellular solutions. Cells in which holding current changed or access resistance changed by more than 20% between control and test conditions were excluded from analysis.

Whole-cell recordings

Whole-cell recordings were made from XII MNs in rhythmically-active medullary slices and non-rhythmic slices. Patch pipettes (3–5 MΩ) were pulled on a horizontal puller (P-97, Sutter Instrument, Novato, CA, USA) from filamented borosilicate glass (1.2 mm o.d., Harvard Apparatus, Edenbridge, UK). For experiments on inspiratory XII MNs, pipettes were filled with solution containing (in mM) either: 140 potassium gluconate, 5 NaCl, 1 $CaCl_2$, 1 $MgCl_2$, 10 EGTA, 10 Hepes (liquid junction potential: −12.5 mV), and 1 glucose, or 20 potassium gluconate, 10 NaCl, 10 Hepes, 2 $MgCl_2$, 30 K_4-BAPTA (liquid junction potential: −18.8 mV). For experiments examining the putative modulation of I_{CAN} by $P2Y_1$Rs in XII MNs of quiescent slices, three different Cs^+-based intracellular solutions were used that contained (in mM): (1) 135 CH_3O_3SCs, 5 NaCl, 1 $MgCl_2$, 10 Hepes, 0.2 EGTA (liquid junction potential: −8.2 mV); (2) low-BAPTA solution: 135 CH_3O_3SCs, 5 NaCl, 2 $MgCl_2$, 0.2 $CaCl_2$, 10 Hepes, 2 Cs_4-BAPTA (liquid junction potential: −8.7 mV); (3) high-BAPTA solution: 20 CH_3O_3SCs, 10 NaCl, 2 $MgCl_2$, 10 Hepes, 30 Cs_4-BAPTA (liquid junction potential: −18.2 mV). Membrane potentials were not adjusted to correct for liquid junction potentials. High BAPTA was used to produce a time-dependent inhibition of I_{CAN}. With increased time in the whole-cell configuration and progressive dialysis, intracellular BAPTA concentration and calcium buffering capacity increased, progressively attenuating the calcium transients necessary for activation of I_{CAN}. Low BAPTA solution was used as a control for high BAPTA. Osmolarity of all intracellular solutions was adjusted to 290–300 mOsm with sucrose and pH to 7.2–7.3 with either KOH or CsOH. The effects of high BAPTA were assessed by comparing responses evoked immediately after obtaining the whole-cell configuration (first 2 min) with those evoked 15–20 min later.

Unless stated otherwise, the PIC was measured by applying three, consecutive slow depolarizing ramps (−80 mV to 0 mV, 14 mV s^{-1}, 40 s between ramps). The current responses to the voltage ramps were low-pass filtered (Hamm *et al.* 2010) and then averaged. Leak conductance (g_L) was calculated from the line of best fit between current and voltage over the linear range between −80 and −65 mV (i.e. before activation of inward currents) and subtracted from the whole-cell current. PIC amplitude was measured from the leak-subtracted currents, as described previously (Lamanauskas & Nistri, 2008; Bellingham, 2013).

Drugs and their application

All drugs were dissolved in standard aCSF, with the exception of flufenamic acid (FFA) and 9-phenanthrol, which were dissolved in dimethyl sulphoxide (DMSO) and then diluted ×1000 in aCSF to a final concentration of 0.1 mM before use. Drugs used included: γ-aminobutyric acid (GABA), a $GABA_A$ and $GABA_B$ receptor agonist (1 mM, Sigma, St. Louis, MO, USA); 2-methylthioadenosine 5′-diphosphate (2MeSADP), a $P2Y_{1,12,13}$R agonist (0.1–10 mM, Sigma); (*N*)-methanocarba-2MeSADP (MRS2365), a $P2Y_1$R agonist (0.01–1 mM, Tocris, Bristol, UK); L-glutamic acid (glutamate), a general glutamate receptor agonist (0.1 mM, Sigma); FFA, an I_{CAN} antagonist (0.1 mM, Sigma); tetrodotoxin (TTX, 0.5 or 1 μM, Alomone Labs, Jerusalem, Israel); and 9-phenanthrol, a TRPM4 blocker (0.1 mM, Sigma).

Drugs were either applied to the bath or applied locally via pressure ejection from triple-barrelled pipettes pulled from borosilicate glass capillaries (cat no. 3B120F-4, WPI,

Sarasota, FL, USA). For nerve recording experiments, drug pipettes were placed at the site at which local application of GABA produced maximum inhibition of inspiratory output (see Results). For whole-cell recording experiments, triple-barrelled drug pipettes were placed superficial to the surface of the slice approximately 25–50 μm upstream of the MN soma. A minimum of 15 min was allowed between consecutive P2R agonist applications because responses are consistent when evoked at this interval (Huxtable *et al.* 2009, 2010).

Immunohistochemistry

Neonatal rats (P0–P3) were anaesthetized deeply with isoflurane and perfused transcardially with cold phosphate buffer (0.1 M PB) followed by 4% paraformaldehyde in PB. Brainstems were removed, postfixed overnight in 4% paraformaldehyde, and sliced into 50 μm transverse sections on a Leica VT 1000S vibratome. Sections were stored in 0.01% sodium azide in PB until processed.

The pattern of $P2Y_1R$ expression in XII MNs in relation to NK1R (receptor for the neuromodulator substance P) and choline acetyl transferase (ChAT, a MN marker) expression was examined via immunohistochemistry using the TSA Fluorescein System protocol (NEL701A, PerkinElmer, Boston, MA, USA). The rabbit anti-$P2Y_1R$ antibody (Alomone Labs) was used first, followed by the rabbit anti-NK1R antibody (Advanced Targeting Systems, San Diego, CA, USA) combined with a goat anti-ChAT antibody (Chemicon, Temecula, CA, USA).

In brief, free-floating sections were initially washed three times with 0.1 M phosphate-buffered saline (PBS) for 15 min. Endogenous peroxidase activity was quenched by 20 min incubation with 1% H_2O_2. All washes mentioned in the following text similarly comprised three washes of 15 min each. All incubations were performed on an oscillating shaker at room temperature. After PBS washes, sections were placed in 0.3% Triton X-100 in TNB (0.1 M Tris-HCl, pH 7.5, 0.15 M NaCl, 0.5% blocking reagent, supplied in kit) buffer for 1 h to decrease non-specific staining and increase antibody penetration. Sections were then incubated in the first primary antibody (rabbit anti-$P2Y_1R$ antibody; 1:30,000) and 0.3% Triton-X100 in TNB buffer overnight (14–16 h). After this first primary antibody incubation, sections were washed in TNT (0.1 M Tris-HCl, pH 7.5, 0.15 M NaCl, 0.05% Tween 20) buffer and incubated with biotin-conjugated AffiniPure donkey anti-rabbit IgG (H–L) (1:200; Jackson ImmunoResearch Laboratories, West Grove, PA, USA) in TNB buffer for 2 h. After washes in TNT buffer, sections were incubated with streptavidin–HRP (1:150) for 1 h, washed in TNT buffer, incubated for 10 min in TSA Fluorescein System Amplification Diluent (1:75), and washed again in TNT buffer.

In preparation for the application of the second and third primary antibodies, sections were again blocked in TNB buffer. Sections were then incubated overnight in the second (rabbit anti-NK1R antibody; 1:1000) and third (goat anti-ChAT; 1:300) primary antibodies, washed in TNT buffer, incubated for 2 h with secondary antibodies conjugated to fluorescent probes for both primary antibodies (NK1R, 1:400, Cy3-conjugated AffiniPure donkey anti-rabbit IgG (H–L), Jackson ImmunoResearch Laboratories; ChAT, 1:400, Cy5-conjugated donkey anti-goat IgG, Jackson ImmunoResearch), washed again in TNT buffer and PBS, and then mounted on slides and coverslipped with Fluorosave Reagent (Calbiochem, San Diego, CA, USA). Control sections were processed in an identical manner with the exception that the primary antibody was omitted from the incubation step. Since both $P2Y_1$ and NK1R antibodies were generated in rabbit, we included an additional control to ensure that there was no cross-reactivity between the NK1R secondary antibody and the $P2Y_1$ primary antibody. Sections were first incubated in the $P2Y_1R$ primary antibody, then the $P2Y_1R$ secondary antibody, followed by the NK1R secondary antibody. Sections were devoid of NK1R secondary antibody (Cy3) labelling, confirming a lack of cross-reactivity.

Immunofluorescence images (1024 × 1024 pixels) were acquired with a Zeiss (Oberkochen, Germany) LSM510 confocal laser-scanning system using an Axiovert 100M microscope and the following objectives: Fluar ×10 (NA 0.5), Fluar ×20 (NA 0.75), or Plan- Neofluar ×40 (NA 1.3). Images were exported to Adobe Photoshop, version 7.0, and adjusted for contrast and brightness.

Laser-capture microdissection and PCR

Tissue collection and sectioning. Neonatal (P3) and juvenile (P14) rats were anaesthetized with isoflurane and brainstems removed rapidly into ice-cold, sterile aCSF. For tissue punches, the medulla was blocked, glued to the vibratome chuck and 300 μm-thick transverse sections were cut serially on a vibratome. Sections were laid out sequentially, transilluminated and sections containing the XII nuclei or preBötC selected. XII and preBötC tissue was harvested using 19 and 21 gauge tissue punches, respectively (Huxtable *et al.* 2009). Two punches from each animal were put directly into lysis buffer (Dynabead mRNA DIRECT kit; Invitrogen Molecular Probes, Carlsbad, CA, USA) and stored at −80°C until needed. mRNA was extracted using the Dynabead mRNA DIRECT kit (Invitrogen Molecular Probes). Because preBötC neurons show an I_{CAN} current (Funk *et al.* 1997; Pace *et al.* 2007; Mironov, 2008) and preBötC tissue expresses transcripts for TRPM4 and TRPM5 (Crowder *et al.* 2007), preBötC punches were used as

a positive control. mRNA was extracted using the same Dynabead mRNA DIRECT kit (Invitrogen Molecular Probes). mRNA was used as the template to make cDNA using the High Capacity Reverse Transcription kit (Applied Biosystems, Carlsbad, CA, USA) with oligo d(T) primers. The product of the reverse transcription reaction was then cleaned using MinElute PCR purification kit (Qiagen, Mississauga, Ontario, Canada) to obtain a pure and concentrated sample that was used directly in the real-time PCR reaction (see below).

Laser-capture microdissection (LCM) of XII MNs. The brainstem was blocked with a small segment of spinal cord attached to facilitate tissue manipulation. The tissue was placed in a cryomould (on a bed of dry ice) and oriented for sectioning in the transverse plane. The cryomould was then filled with Tissue-Tek (Sakura Finetek, Torrance, CA, USA), which solidified within 1 min, and stored at −80°C until needed. Brainstems were transversely sectioned in the caudal-to-rostral direction using a cryostat (Leica CM 1850) set at −20°C. Sections were cut at 20 μm thickness (and tissue discarded) until the caudal margin of the XII nucleus was evident. At this point, thickness was reduced to 6 μm and sections were placed on Fisherbrand Superfrost (Fisher Scientific, Ottawa, ON, Canada) microscope slides. Slides were kept in the cryostat (−20°C) for ∼15 min, and then stored at −80°C until LCM was performed. Approximately 60 slides, each containing two or three sections (this minimized freeze–thaw cycles and reduced RNA degradation), were collected from each of two P3 rats (each rat was from a different litter).

Tissue preparation for LCM. Sections were stained and dehydrated according to the Arcturus LCM Histogene Frozen Section Staining Kit protocol (Arcturus Bioscience, Mountain View, CA, USA). Two slides were removed from −80°C, defrosted for 10 s, and placed sequentially in reaction tubes containing 75% ethanol (15 s), water (15 s), cresyl violet (15–30 s), water (quick dip), 75% ethanol (30 s), 95% ethanol (30 s), 100% ethanol (2 × 1 min), xylene (1 min) and finally a second xylene tube where slides were stored until LCM.

Laser-capture microdissection. Microscope slides were placed one at a time on the stage of the Arcturus Autopix LCM (Arcturus Bioscience). A roadmap image of the entire slice was first taken at ×4 magnification, followed by higher magnification (×20) images of the left and right XII nuclei that were used to select MNs and guide LCM. An HS LCM cap was then placed over the tissue and laser settings adjusted to produce a laser spot size of 15 μm (power 80–85 mW, 200 mV per target, pulse duration 1800–1950 μs, automatic double-pulse), which fell completely inside the MN borders. MNs were selected all at once based on size and morphology. Automated dissection was then initiated. All MNs were captured within 1.5 h from starting the dehydration process. MNs surrounded by fractured tissue were not selected because dissecting such sites would often capture tissue outside the boundaries of the MN. Images of the dissected field were taken before and after dissection and also of the cap containing dissected cells (the Arcturus phototriad, Fig. 9*B*). The number of targeted MNs was compared with the number captured. Twenty to 100 MNs were captured per section and approximately 500 MNs captured from two P3 animals. In all successful runs, laser capture efficiency was 100%; i.e. every targeted MN was captured. Noteworthy is that unsuccessful runs were always 100% unsuccessful. Use of a new cap on the same tissue slice typically resolved the problem.

Following laser dissection and capture, each HS LCM cap was examined under a microscope (×20) and discarded if cellular debris or foreign particles were evident. mRNA was extracted using the Arcturus PicoPure RNA Isolation kit. mRNA from each animal was pooled from multiple caps (∼100 neurons) and reverse transcription (RT) performed with an Applied Biosystems (ABI, Burlington, ON, Canada) High Capacity Reverse Transcription kit using oligo d(T) primers. cDNA was stored at −80°C. Samples were not treated with DNase due to small amounts of mRNA and the risk of degradation (Nolan *et al.* 2006). A no-RT control was used to test for cross-contamination of genomic DNA, while a no-template control, in which water was added in place of cDNA, was used to test for contamination.

Real-time PCR. The Bio-Rad (Hercules, CA, USA) iCycler and Applied Biosystems 2x SYBR Green Master Mix were used to run the PCR. Genes of interest were *TRPM4* and *TRPM5*. The housekeeping gene encoding *cyclophilin A* was used to control for variations in quality and quantity of cDNA between different samples. For *TRPM4*, the forward and reverse primer codes were 5′-AGTTGAGTTCCCCCTGGACT-3′ and the 5′-AATTCCAGTCCCTCCCACTC-3′, respectively, making a 148 bp amplicon. For *TRPM5*, forward and reverse primer sequences were 5′-CATCTCCTTCAGTG AGGATGC-3′ and 5′-CTTC TCCAATT GGCCACCAT-3′, making a 115 bp amplicon. Standard primers were used for *cyclophilin A*. Primers were designed to span an exon–exon junction to further reduce the possibility of amplifying genomic DNA. Real-time PCR reaction conditions were as follows: 12 μl of ABI 2x SYBR Green buffer, 0.25 μl of Amp Erase, 0.05 μl of forward primer, 0.05 μl of reverse primer and 1 μl of cDNA (50 ng μl^{-1}) for a total reaction volume of 25 μl. Temperature curves were generated for each gene of interest to test for primer dimers. Primer efficiencies were all verified at greater than 98%; each sample was run in triplicate, including standards for each transcript, to

obtain validated concentration curves (cycle number *vs.* cDNA copy number).

Data analysis

Parameters are reported in absolute terms, or relative to control (pre-drug or prestimulus) levels, as mean ± standard error of the mean (SEM). Comparisons between groups were performed on raw data. Student's *t* test (paired or unpaired as dictated by the data) was used to compare two groups, while analysis of variance (ANOVA) was used in conjunction with Bonferroni correction for multiple comparisons or Newman–Keuls *post hoc* test (Prism 4.2, GraphPad Software, San Diego, CA, USA) to compare three or more groups. *P* values less than 0.05 were considered significant.

Results

P2YR activation in phrenic and XII nuclei

To test the hypothesis that phrenic and XII nuclei are sensitive to P2YR modulation, we compared the effects on inspiratory burst activity of locally applying P2YR agonists over the C4 spinal cord of the BSSC preparation and the XII nucleus of the rhythmic slice preparation. Valid comparison required verification that locally applied drugs had equal access to the two MN pools. To address this issue, we compared the effects of GABA (1 mM, 30 s) on C4 (Parkis *et al.* 1999) and XII inspiratory burst amplitudes (Marchetti *et al.* 2002; van Brederode *et al.* 2011). For the XII applications, the drug pipette was placed just below the slice surface in the ventromedial portion of the nucleus. GABA was applied. The pipette was then systematically moved in the transverse plane and the GABA application repeated at 5 min intervals to identify the site of maximum effect. For injections over the phrenic MN pool at C4, the pia mater was gently removed while monitoring C4 output for reductions in burst amplitude indicative of damage to the MNs. Data were excluded from analysis if removal of the pia caused amplitude to fall more than 10%. Note that GABA had very little effect on C4 burst amplitude prior to removing the pia mater. Then, as with XII injections, pipette position was systematically changed to identify the site of maximum GABA sensitivity. Once identified, all subsequent injections were made at the same site. Only two concentrations of 2MeSADP were used in any single experiment because one of the three pipette barrels contained GABA, leaving two barrels for the P2YR agonists.

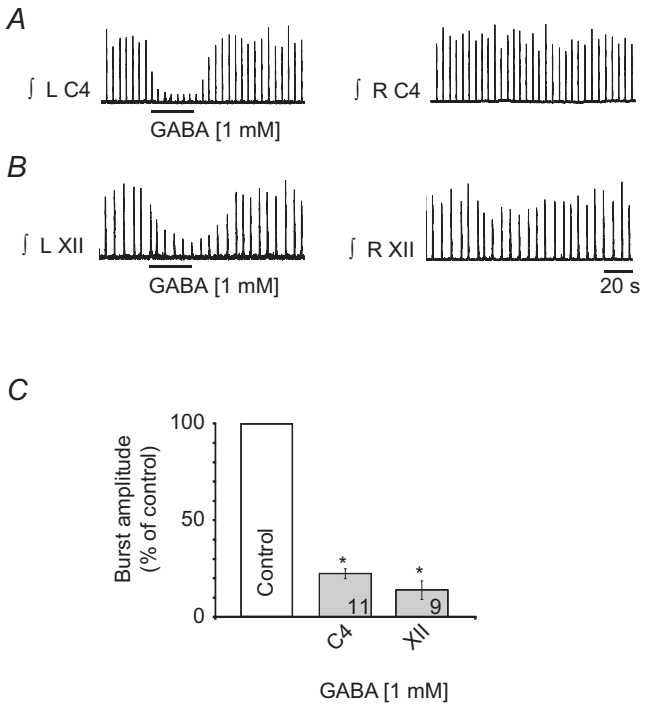

Figure 1. GABA is equally effective at inhibiting inspiratory burst amplitude in C4 and XII MN pools
Rectified, integrated recordings from left (L) and right (R) C4 (*A*) and XII (*B*) nerve rootlets showing the ipsilateral burst amplitude depression produced by a 30 s injection of 1 mM GABA over each MN pool that was used to identify the site for P2Y agonist application. *C*, group data; numbers for each group are in the bottom of each column. *Significant difference from control; $P < 0.05$ (*post hoc* analysis, Bonferroni method).

As shown in the nerve recording traces for a single BSSC and slice preparation (Fig. 1*A* and *B*) and group data (Fig. 1*C*), GABA caused similar reductions in C4 and XII inspiratory burst amplitudes to 22 ± 3 ($n = 11$, $P < 0.05$) and 14 ± 5% ($n = 9$, $P < 0.05$) of control. Only those preparations in which GABA reduced burst amplitude to at least 35% of control were used.

We first tested the effects of P2YR activation on inspiratory motor output by locally applying the P2YR agonist 2MeSADP (Chhatriwala *et al.* 2004; Carrasquero *et al.* 2005; León *et al.* 2006; Kahlert *et al.* 2007; Ortega *et al.* 2008). The response of C4 and XII nuclei to 2MeSADP comprised a tonic excitation, apparent as a thickening and upward shift in the baseline of the integrated nerve recordings, and a superimposed increase of the inspiratory burst amplitude (Fig. 2*A* and *B*). The response was relatively slow in onset compared to that evoked by the general P2R agonist ATP (Funk *et al.* 1997; Miles *et al.* 2002), peaking in the second half of the 60 s injection. The effects of 2MeSADP on the C4 nerve activity were exclusively ipsilateral, whereas a small contralateral effect was observed during XII injections in 2 of 30 preparations, probably reflecting the proximity of the contralateral XII nucleus and minimal diffusion barrier compared to the phrenic nucleus. While the responses of C4 and XII MN pools to 2MeSADP were qualitatively similar, the XII MN pool was significantly more sensitive (Fig. 2*C*). At the phrenic MN pool, 10 mM 2MeSADP evoked minor tonic discharge and a 25 ± 5% potentiation of inspiratory burst

amplitude (Fig. 2*A* and *C*, $n = 11$, $P < 0.05$). Lower concentrations had no effect.

In contrast, in the XII nucleus, 0.1 mM and 1 mM 2MeSADP generated robust, dose-dependent increases in tonic activity and burst amplitude. At 0.1 mM 2MeSADP, the tonic discharge was accompanied by a 52 ± 13% ($n = 7$) increase in XII inspiratory burst amplitude (Fig. 2*C*). After correcting for the baseline shift associated with the tonic activity, the amplitude potentiation of 80 ± 21% ($n = 9$) evoked by 1.0 mM 2MeSADP in the XII nucleus was not statistically greater than the effect of 2MeSADP at 0.1 mM, but it was significantly greater than the response evoked in the phrenic nucleus by 1.0 mM 2MeSADP. At 10 mM, the increase in XII tonic activity was so large that it obscured inspiratory burst activity (data not shown).

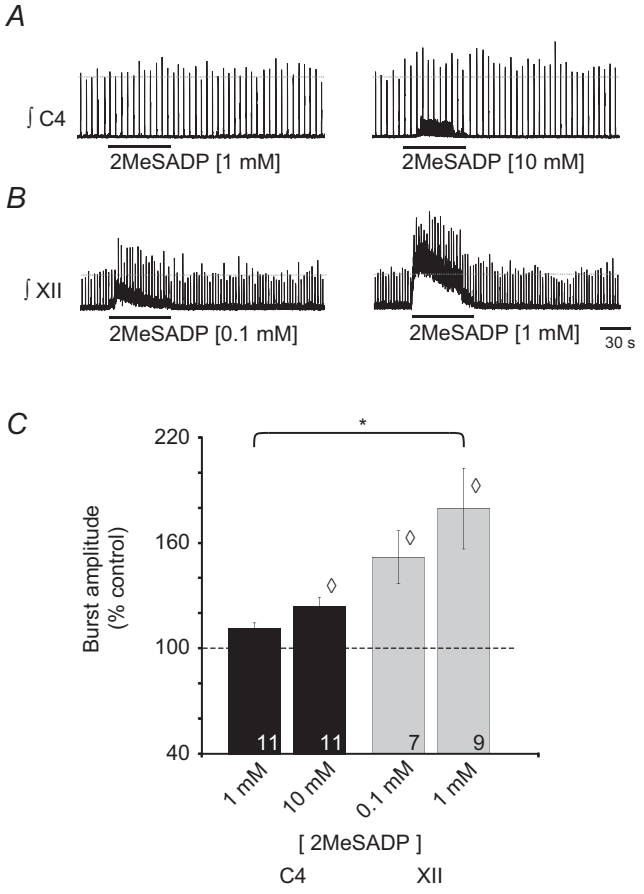

Figure 2. P2YR activation potentiates inspiratory burst amplitude in C4 and XII MN pools
Rectified, integrated recordings from C4 (*A*) and XII (*B*) nerve rootlets, illustrating the burst amplitude potentiation produced by a 60 s injection of 2MeSADP, a P2Y agonist, over the C4 and XII MN pools. *C*, group data showing increase in burst amplitude evoked by 2MeSADP. Numbers for each group are in the bottom of each column. Dotted line indicates control levels (100%); ◊ indicates significant difference from control; * indicates significant difference between 2MeSADP (1 mM) in C4 and XII pools; $P < 0.05$ (*post hoc* analysis, Bonferroni method).

$P2Y_1R$ activation in phrenic and XII nuclei

2MeSADP is an agonist at $P2Y_1$, $P2Y_{12}$ and $P2Y_{13}$Rs (Chhatriwala *et al.* 2004; Carrasquero *et al.* 2005; Kahlert *et al.* 2007; Ortega *et al.* 2008). To further delineate receptor subtype, we assessed the sensitivity of phrenic and XII MN pools to the $P2Y_1R$ agonist MRS2365, which has a 4-fold greater affinity for $P2Y_1$Rs than 2MeSADP, no agonist or antagonist activity at $P2Y_{12}$Rs and is >10,000-fold more selective for $P2Y_1$ compared to $P2Y_{13}$Rs (Chhatriwala *et al.* 2004; Jacobson *et al.* 2006). We focused on $P2Y_1$Rs due to their dominant role in the ATP-mediated excitation of preBötzinger complex (preBötC) inspiratory rhythm-generating networks (Lorier *et al.* 2007).

In the C4 nucleus, 0.1 and 1 mM MRS2365 potentiated inspiratory burst amplitude by 12 ± 3% and 25 ± 7% ($n = 8$), respectively (Fig. 3*C*, $P < 0.05$). MRS2365 had a relatively minor effect on C4 tonic discharge; it was observed in only 1 of 8 preparations at 0.1 mM and 2 of 8 preparations at 1.0 mM (Fig. 3*A*). When applied to XII nuclei, again at 10-fold lower concentrations than at C4, 0.01 and 0.1 mM, MRS2365 increased inspiratory burst amplitude by 45 ± 7% and 60 ± 9% ($n = 21$), respectively (Fig. 3*C*, $P < 0.05$). MRS2365-evoked increases in tonic activity were observed in 13 of 21 preparations at 0.01 mM and 14 of 21 preparations at 0.1 mM (Fig. 3*B*).

In summary, the inspiratory and tonic activity of both phrenic and XII MN pools are sensitive to P2YR modulation. The $P2Y_1R$ agonist MRS2365 appears to preferentially potentiate inspiratory over tonic activity, and XII MN activity is significantly more sensitive to P2YR modulation than phrenic MN activity.

Mechanisms underlying the P2YR-mediated modulation of XII MN activity

Site of action: pre- *vs.* postsynaptic mechanisms. C4 activity was only sensitive to P2YR agonists at very high concentrations. We therefore focused on XII MNs to elucidate the mechanisms by which P2YR signalling modulates MN excitability. We began with a generic analysis of P2YR effects due to the greater sensitivity of whole-cell recording methods to detect small, subthreshold effects that may be mediated by other P2YR subtypes. We locally applied the endogenous agonists ADP, which binds to $P2Y_{1,6,12,13}$Rs, and uridine triphosphate (UTP), which activates $P2Y_{2,4,6}$Rs (von Kugelgen, 2006). Importantly, aside from weak actions of UTP on $P2X_3$Rs (Rae *et al.* 1998), and ADP on $P2X_7R$, neither ADP nor UTP activate P2XRs. Under voltage-clamp recording conditions ($V_h = -60$ mV), UTP (0.1 mM, $n = 4$; 1.0 mM, $n = 3$) had no effect on membrane current of inspiratory XII MNs (Fig. 4*A*). Similarly, 1.0 mM ADP had no effect on baseline membrane current of XII MNs recorded in non-rhythmic slices (Fig. 4*B*, left panel; $n = 3$). Given

the suggestion from nerve recording experiments (Fig. 3) that $P2Y_1R$ activation may potentiate synaptic inputs and that degradation of ADP by ectonucleotidases may obscure its action (Zwicker *et al.* 2011), we increased ADP concentration to 10 mM in two experiments (Fig. 4*B*, right panel). In both MNs, 10 mM ADP caused an increase in the frequency and amplitude of the inward synaptic currents. This increased synaptic activity was superimposed on a slow, inward DC current that averaged -18 ± 8 pA (Fig. 4*B*, right panel, and *D*, $n = 2$). Neither 1.0 ($n = 6$) nor 10 mM ($n = 4$) ADP had a significant effect on membrane current following bath application of 0.5 μM TTX (Fig. 4*C* and *D*).

We next used rhythmic medullary slices and the specific $P2Y_1R$ agonist MRS2365 to test the hypothesis that $P2Y_1R$ activation potentiates inspiratory and non-inspiratory synaptic inputs to XII MNs. Local application of MRS2365 at 0.1 and 1.0 mM over the XII nucleus increased the peak amplitude of inspiratory synaptic currents by $19 \pm 5\%$ ($n = 8$) and $19 \pm 3\%$ ($n = 8$), respectively (Fig. 5, $P < 0.05$). The similarity of response at both concentrations suggests that the effect was saturated at the lower concentration. Similarly, the effect of MRS2365 on the charge transfer per inspiratory current (i.e. area under the current *vs.* time plot), was a $20 \pm 10\%$ and $22 \pm 7\%$ potentiation at 0.1 and 1.0 mM MRS2365, respectively. We also examined the effects of MRS2365 on the non-inspiratory synaptic activity (i.e. that occurring during the interval between inspiratory bursts) that was superimposed on a slow inward current (see also Fig. 6*A* and *B*). Postsynaptic current (PSC) activity in the 2 min prior to MRS2365 application was compared to that during the 1 min encompassing the peak of the response. PSC amplitude was minimally affected by 0.1 mM MRS2365 (-37 ± 4 pA

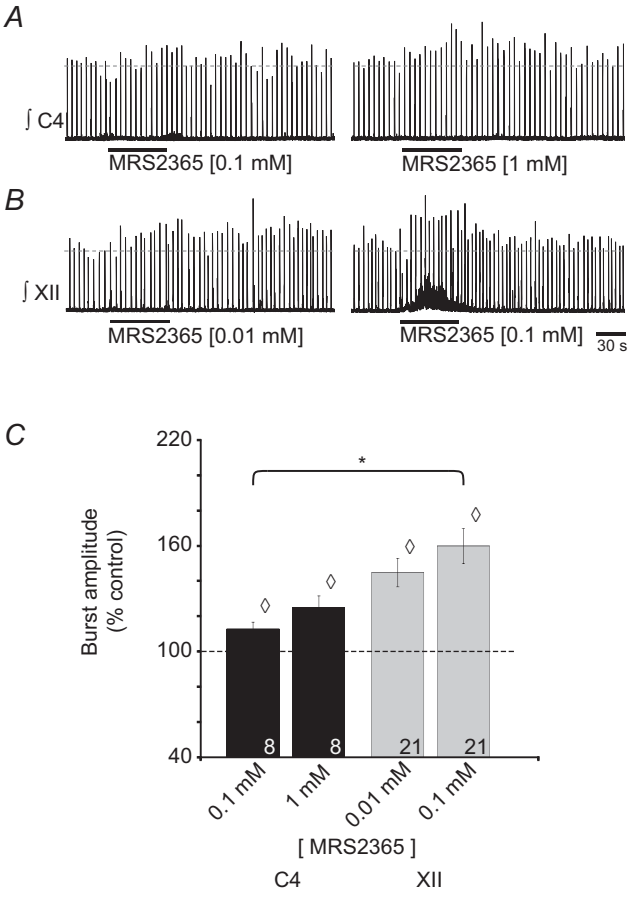

Figure 3. The $P2Y_1R$ agonist MRS2365 potentiates inspiratory burst amplitude at C4 and XII nuclei
Rectified, integrated recordings from C4 (*A*) and XII (*B*) nerve rootlets, showing the burst amplitude potentiation produced by a 60 s injection of MRS2365, a $P2Y_1R$ agonist, over the phrenic and XII MN pools. *C*, group data showing the effect of MRS2365 on inspiratory burst amplitude. Numbers for each group are in the bottom of each column. Dotted line indicates control levels (100%); ◊ indicates significant difference from control; * indicates significant difference between MRS2365 (0.1 mM) in C4 and XII pools; $P < 0.05$ (*post hoc* analysis, Bonferroni method).

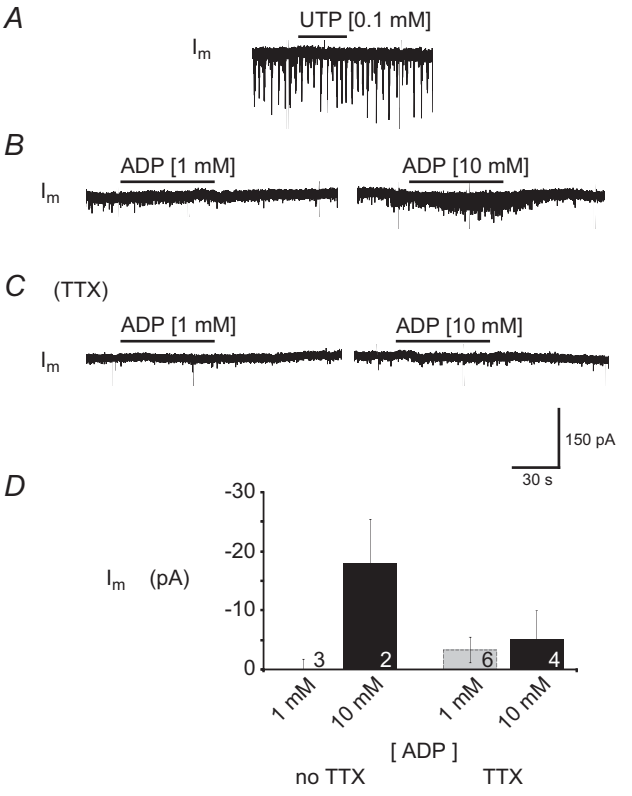

Figure 4. XII MNs are insensitive to P2YR agonists UTP and ADP
Whole-cell voltage-clamp recordings from XII MNs held at –60 mV demonstrating the effects produced by a 60 s UTP (*A*) and ADP application in the absence (*B*) and in the presence (*C*) of TTX (0.5 μM). *D*, group data showing effects of ADP on membrane current (I_m). Numbers for each group are in the bottom of each column; results from 1 mM and 10 mM ADP injections were not significantly different, in either absence or presence of TTX (0.5 μM); $P > 0.05$ (one-way ANOVA).

in control *vs.* −40 ± 4 pA in MRS2365; an insignificant 6 ± 3% change, $n = 8$). At 1.0 mM, MRS2365 increased PSC amplitude from −37 ± 3 to −53 ± 7 pA (39 ± 10%, $n = 8$, Fig. 6*A*–*C*). PSC frequency increased by 133 ± 52% and 466 ± 171% of control in response to 0.1 and 1.0 mM MRS2365, respectively (Fig. 6*A*, *B* and *D*, $P < 0.05$). Finally, the DC current evoked by 0.1 and 1.0 mM MRS2365 averaged −9 ± 3 pA and −25 ± 7 pA (Fig. 6*A*, *B* and *E*; $n = 8$).

The effects of MRS2365 on PSC amplitude and frequency suggested pre- and postsynaptic actions. To determine the potential site(s) of action, we examined the effects of MRS2365 on the amplitude and frequency of miniature postsynaptic currents (mPSCs) 2 min prior to drug application and at minutes 2–4 when the control response to MRS2365 (i.e. that observed prior to TTX application) was maximal. mPSCs were analysed in five XII MNs. As seen in response to ADP (Fig. 4), activation of $P2Y_1$Rs in the presence of bath-applied TTX had no

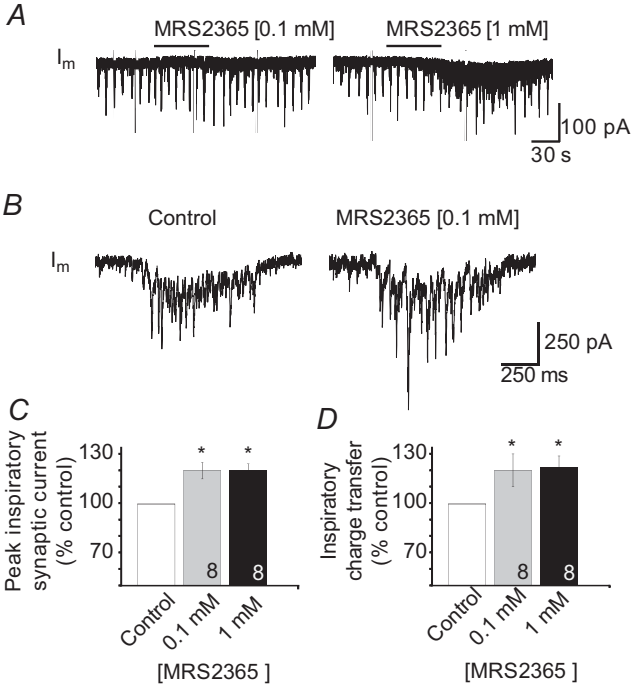

Figure 5. $P2Y_1$R activation potentiates inspiratory synaptic currents
A, long time-series whole-cell voltage-clamp recordings from an inspiratory XII MN held at –60 mV illustrating the effects on inspiratory synaptic currents of MRS2365 locally applied at 0.1 and 1 mM (60 s). *B*, inspiratory synaptic current averaged from six consecutive inspiratory cycles in control (left) and during the peak of the response to MRS2365 (60 s, 0.1 mM). *C*, group data showing the MRS2365-mediated potentiation of inspiratory synaptic currents. Data are reported relative to control as the peak current and charge transfer per inspiratory burst. Numbers for each group are in the bottom of each column; * indicates significant difference from control, $P < 0.05$ (*post hoc* analysis, Bonferroni method).

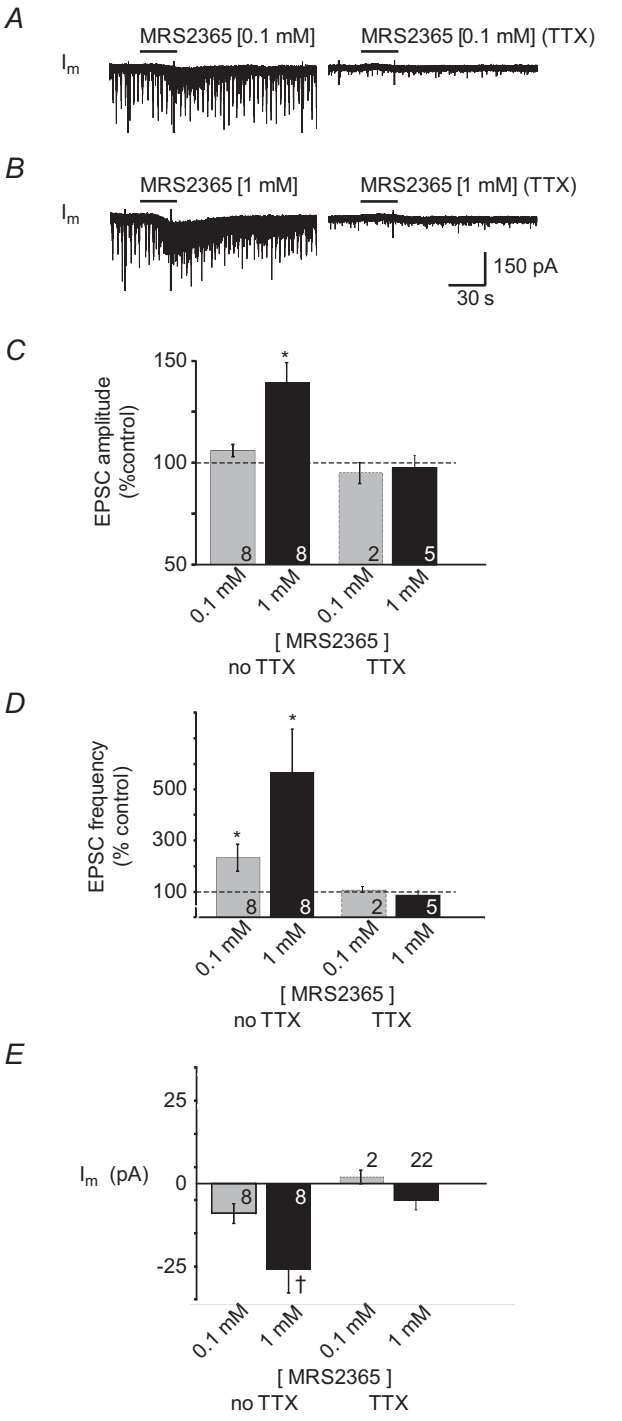

Figure 6. MRS2365 potentiates synaptic activity before but not after application of TTX
Whole-cell voltage-clamp recordings from an inspiratory XII MN showing the effects of MRS2365 locally applied at 0.1 mM (*A*) and 1 mM (*B*) before (left) and after (right) bath application of 0.5 μM TTX. Group data show changes in EPSC or mEPSC (in TTX) amplitude (*C*), EPSC or mEPSC frequency (*D*) and membrane current (*E*) evoked by MRS2365 injections depicted in *A* and *B*. Numbers for each group are in the bottom of each column; * indicates significant difference from control; † indicates significant difference from MRS2365 (0.1 mM); $P < 0.05$ (*post hoc* analysis, Bonferroni method).

significant effect on PSC amplitude or frequency (Fig. 6). MRS2365 was also without effect on membrane current. In TTX, only 3 of 22 XII MNs showed a postsynaptic inward current in response to 1 mM MRS2365 (average of -39 ± 6 pA, $n = 3$). Overall, in TTX, MRS2365 had no significant effect on synaptic inputs or membrane current in XII MNs held at -60 mV.

$P2Y_1R$ immunolabelling. Due to the lack of an obvious pre- or postsynaptic effect of MRS2365 on XII MNs in TTX, we used an immunohistochemical approach to determine if XII MNs express $P2Y_1Rs$. Tissue was simultaneously processed for ChAT immunoreactivity to positively identify MNs and NK1R immunoreactivity to provide an approximate reference for receptor labelling intensity. In neonatal rats, NK1R expression is strong in XII MNs and substance P is a potent modulator of XII MN activity (Yasuda *et al.* 2001). Tissue processed from four rats revealed that while immunolabelling for $P2Y_1R$ appeared weaker than for NK1R, the majority of ChAT-labelled neurons in the XII nucleus showed $P2Y_1R$ immunoreactivity (Fig. 7).

Presence of I_{CAN}. Block of apparent pre- and postsynaptic actions of MRS2365 by TTX led us to hypothesize that MRS2365 potentiates synaptic currents through an indirect mechanism that cannot be detected under voltage-clamp conditions in TTX. I_{CAN} is a non-inactivating current (Partridge *et al.* 1994) that contributes to plateau potentials in lumbar MNs (Perrier & Hounsgaard, 1999) and rostral ambiguus MNs (Rekling & Feldman, 1997), as well as persistent inward currents (PICs) in dorsal gastric MNs (Zhang *et al.* 1995) and spinal interneurons (Dai & Jordan, 2010), and amplifies synaptic currents, including inspiratory synaptic currents, in preBötC inspiratory neurons (Pace *et al.* 2007). This I_{CAN}-mediated amplification requires three components: (i) a second-messenger-mediated potentiation of I_{CAN}; (ii) an inspiratory current sufficient to depolarize the membrane to the threshold for high-voltage activated Ca^{2+} channels, and; (iii) Ca^{2+} influx through voltage-gated Ca^{2+} channels to activate the potentiated I_{CAN}. We speculated that the MRS2365 potentiation of EPSC activity (including inspiratory synaptic currents) in XII MNs reflects a similar mechanism and that there is no effect in TTX because the level of depolarization associated with miniature excitatory postsynaptic currents (mEPSCs) is insufficient to activate voltage-gated Ca^{2+} channels and I_{CAN}.

As an initial step in exploring this hypothesis, we tested electrophysiologically for evidence of a PIC in XII MNs using caesium-based intracellular solution (to minimize delayed rectifier potassium conductance) and a voltage-clamp ramp protocol commonly used to reveal PICs (Powers & Binder, 2003; Lamanauskas & Nistri, 2008). At the PIC threshold, a negative slope conductance was apparent where inward current increased as membrane potential depolarized and driving forces for Na^+ and Ca^{2+} currents decreased. PIC magnitude was measured from the leak-subtracted current (Fig. 8*A*, bottom panel) (Lamanauskas & Nistri, 2008; Bellingham, 2013). PICs have been observed in many MN populations (e.g. lumbar flexor MNs: Schwindt & Crill, 1977; Hounsgaard *et al.* 1988; Hounsgaard & Kiehn, 1989; Hultborn & Kiehn, 1992; dorsal gastric MNs: Zhang *et al.* 1995; rostral ambiguous MNs: Rekling & Feldman, 1997; trigeminal MNs: Hsiao *et al.* 1998; vibrissae MNs: Cramer *et al.* 2007; cervical MNs: Enríquez Denton *et al.* 2012), including XII MNs (Powers & Binder, 2003; Koizumi *et al.* 2008; Lamanauskas & Nistri, 2008; Bellingham, 2013). Forty-seven of 49 XII MNs exhibited a PIC. In a random sample of 6 MNs, the PIC activated at an average membrane potential of -58.3 ± 0.3 mV and reached a peak amplitude of -185 ± 1.0 pA at an average potential of -28.3 ± 0.2 mV.

To test whether I_{CAN} contributed to this PIC, responses to slow voltage ramps applied before and during local application of the I_{CAN} blocker FFA (100 μM) were compared. Control voltage ramps were applied during vehicle injection. Test ramps were applied 40 s after the onset of an FFA application that lasted until the ramps were complete. FFA significantly reduced PIC magnitude to $85 \pm 7\%$ of control (Fig. 8*B*, $P < 0.05$, $n = 4$) without affecting input resistance (vehicle *vs.* FFA, $P > 0.05$, paired *t* test).

PICs in XII MNs consist of a Ca^{2+} and Na^+ component (Powers & Binder, 2003; Lamanauskas & Nistri, 2008; Bellingham, 2013). Since our objective was to explore modulation of a Ca^{2+}-dependent current, I_{CAN}, by $P2Y_1Rs$, we isolated the Ca^{2+}-dependent component of the PIC in all subsequent experiments by blocking the Na^+ component with 1 μM TTX in the bath (Hsiao *et al.* 1997; Lee & Heckman, 2001; Li & Bennett, 2003; Powers & Binder, 2003; Koizumi *et al.* 2008). In TTX, local application of FFA caused a much greater $40 \pm 11\%$ decrease in PIC magnitude from -155 ± 14 to -99 ± 25 pA (Fig. 10*B*, $P < 0.05$).

While FFA at 100 μM is reasonably selective for I_{CAN}, it is difficult to exclude the possibility that some of its actions are through inhibition of voltage-gated Ca^{2+} currents (Shimamura *et al.* 2002). We therefore assessed the effects of high intracellular BAPTA concentration on PIC amplitude. Chelation of intracellular Ca^{2+}, if anything, will increase voltage-gated Ca^{2+} currents by increasing the concentration gradient for Ca^{2+}. In contrast, I_{CAN} will be attenuated or blocked by elevated BAPTA since this will attenuate the increase in intracellular Ca^{2+} that is required for I_{CAN} activation. BAPTA effects were assessed by comparing responses obtained

immediately after achieving whole-cell configuration with those obtained 15 min later. Note that in this case the PIC was measured based on only one ramp due to the potential reduction in PIC amplitude with progressive dialysis. High intracellular BAPTA had no effect on input resistance (183 ± 28 *vs.* 205 ± 26 MΩ, control *vs.* control 15 min later, $P > 0.05$, two-way paired *t* test). However, PIC magnitude significantly decreased by 47 ± 12% of control values after 15 min (Fig. 8*C*, $P < 0.05$).

We then tested the effects of the more selective TRPM4 channel blocker, 9-phenanthrol, on the XII MN PIC, again using the low-BAPTA intracellular solution. TRPM4 is a member of the transient receptor potential family that requires depolarization as well as increased levels of intracellular Ca^{2+} for activation (Ullrich *et al.* 2005). In eight cells, we measured PIC magnitude during slow voltage ramps and then again after 10 min of 9-phenanthrol (100 μM) bath application. 9-Phenanthrol caused a 33 ± 6% reduction in PIC magnitude, from −144 ± 40 to −90 ± 22 pA (Fig. 8*D*, $P < 0.05$), but had no effect on input resistance (223 ± 48 *vs.* 189 ± 30 MΩ, control *vs.* 9-phenanthrol, $P > 0.05$, paired *t* test). Based on the sensitivity of the PIC to FFA, high concentrations of intracellular Ca^{2+} buffer, and the TRPM4 blocker, we conclude that a TRPM4-mediated I_{CAN} contributes to the PIC in XII MNs of neonatal rat pups. We also noticed in some recordings that high BAPTA or 9-phenanthrol caused an apparent increase in the peak outward K^+ current. The underlying mechanism was not explored but it has been noted in hippocampal CA1 neurons that BAPTA may induce outward currents (Lancaster & Batchelor, 2000). This may simply reflect that BAPTA can cause neurons to become more electrotonically compact, increasing input resistance and improving space-clamp.

Finally, we asked if XII MNs express the transcript for TRPM4. We also assessed expression of TRPM5 transcripts which is another candidate for I_{CAN} (Launay *et al.* 2002; Hofmann *et al.* 2003; Montell, 2005; Nilius *et al.* 2005; Ullrich *et al.* 2005). XII MNs from juvenile SD rats (P14) express the transcript for TRPM4 (Funk *et al.* 2011). Whether neonatal XII MNs also express TRPM4 is not known. Similarly, the expression of TRMP5 in XII MNs is not known at any age. We first tested for the presence of TRPM5 transcripts via real-time PCR analysis of mRNA extracted from punches of XII nuclei from juvenile rats. Punches of preBötC were included as a positive control (Crowder *et al.* 2007; Pace *et al.* 2007; Funk *et al.* 2011). Real-time PCR analysis of mRNA isolated from punches of the XII nucleus and preBötC of juvenile rats revealed signals for TRPM5 that were ∼10-fold lower than previously published levels for TRPM4 (Crowder *et al.* 2007; Pace *et al.* 2007; Funk *et al.* 2011). Transcript expression levels are reported relative to *cyclophilin A* (ΔCT = cycle threshold number for TRPM4 – cycle threshold number for *cyclophilin A*) (Fig. 9*A*). Since punches are not pure MN samples, we next laser-capture-microdissected ∼500 XII MNs from two P3 animals. We did not examine TRPM5 expression in laser-captured MNs due to the low level of expression found in tissue punches. The phototriad (Fig. 9*B*) shows the XII nucleus in a counter-stained, 6 μm tissue section from a P3 neonatal rat before (top) and after (centre) laser-capture microdissection as well as the captured MNs (bottom). Real-time PCR confirmed the punch data, revealing TRPM4 transcript in neonatal XII MN samples (Fig. 9*C*). These data provide molecular evidence that the mRNA from TRPM4, a putative molecular substrate for I_{CAN}, is expressed in neonatal XII MNs.

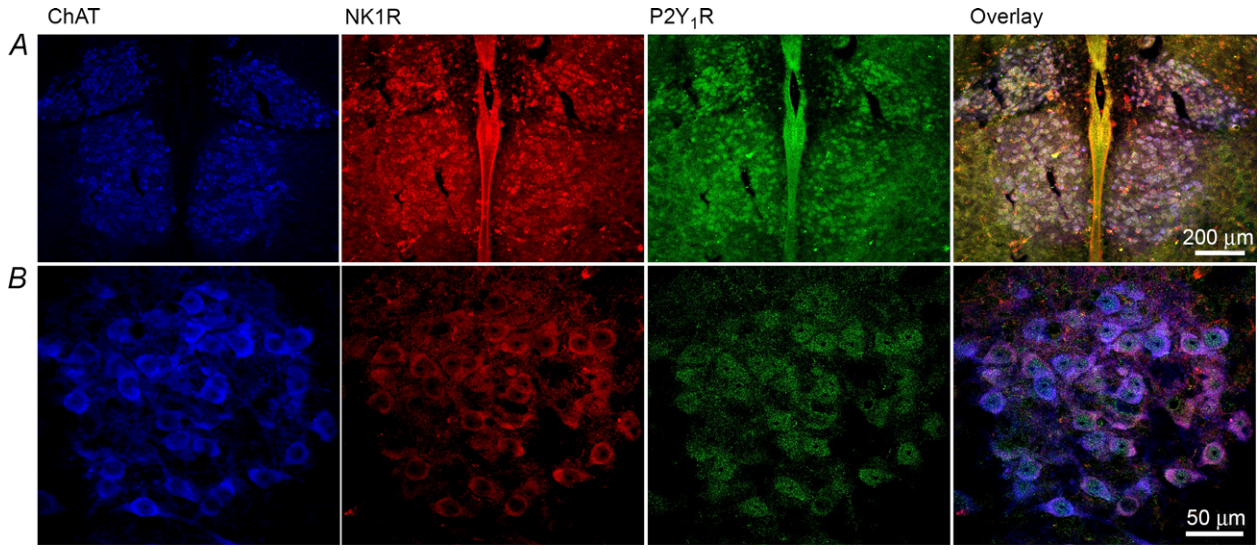

Figure 7. XII MNs show P2Y$_1$R immunolabelling
Low- (*A*) and high-power (*B*) images of the XII nucleus illustrating XII MN immunolabelling for ChAT (blue), NK1R (red), P2Y$_1$R (green) and the overlays of all three images (right panels).

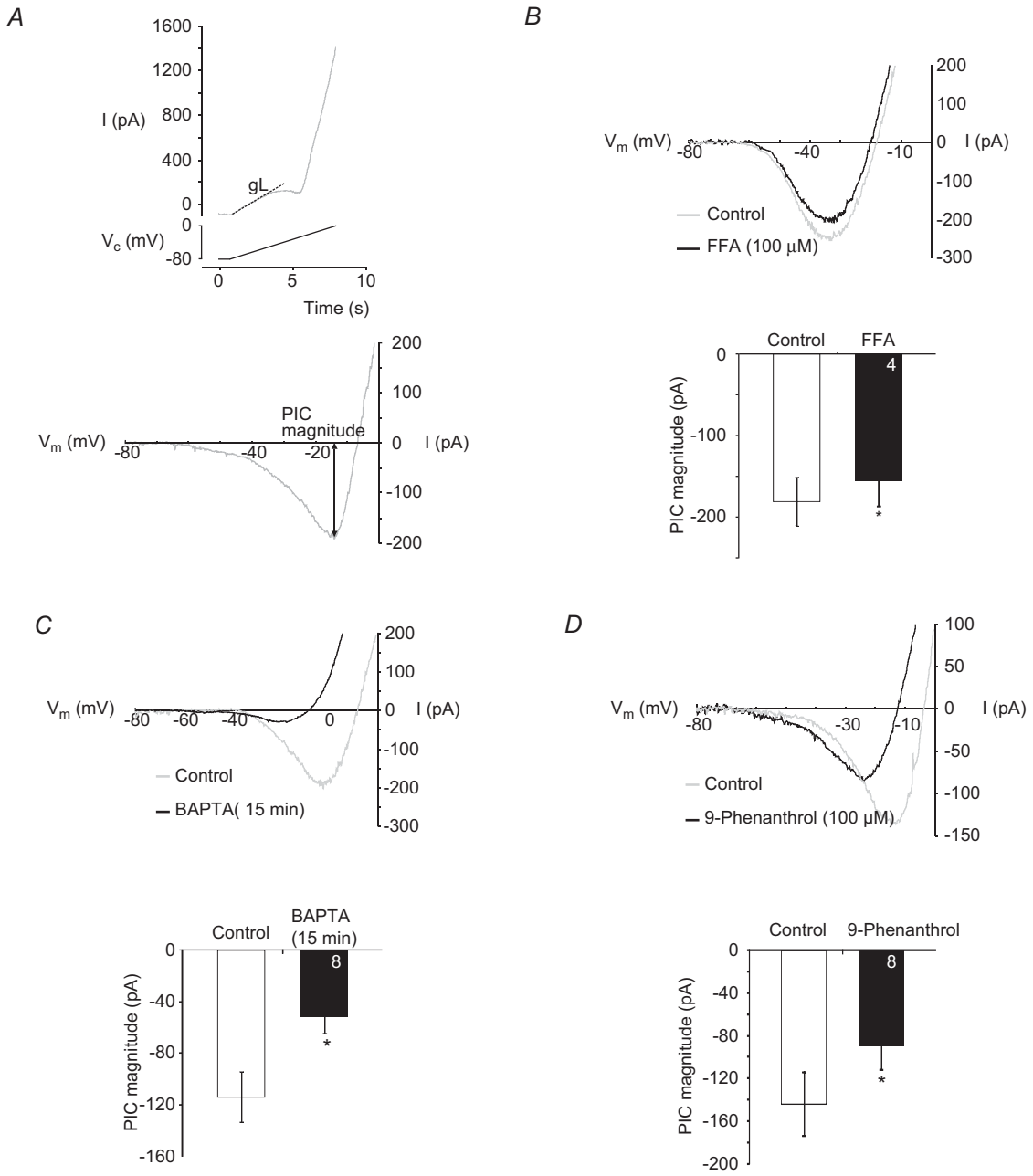

Figure 8. I_{CAN} contributes to the XII MN persistent inward current (PIC)
A, top panel shows filtered current response of a XII MN (top trace) evoked in response to the depolarizing phase of a voltage ramp (from –80 mV to 0 mV, bottom trace). Leak conductance (g_L) (calculated between −80 and −65 mV) is illustrated. Bottom panel illustrates leak-subtracted current and measurement of PIC magnitude. *B*, top: leak-subtracted current responses evoked by the voltage ramp described in *A* during local application of vehicle (control) or FFA, using caesium-based intracellular solution. Bottom: group data showing the peak PIC amplitude in control (open) and FFA (100 μM, filled column). Numbers for each group are in the bottom of each column. $^*P < 0.05$ (one-tailed paired *t*-test). *C*, top: leak-subtracted current responses evoked by voltage ramps during bath application of TTX (1 μM) at the start of the whole-cell recording with caesium-based, high BAPTA intracellular solution (control) and 15 min later (BAPTA). Bottom: group data showing the peak PIC amplitude in control (open) and after 15 min with high BAPTA (filled column). Numbers for each group are in the bottom of each column. ◊, $P < 0.05$ (paired *t* test). *D*, top: leak-subtracted current responses evoked by voltage ramps during control or during bath application of 9-phenanthrol (100 μM), using caesium-based, low-BAPTA intracellular solution. Bottom: group data showing the peak PIC amplitude during bath application of TTX (1 μM) in control (open) and during bath application of 9-phenanthrol (filled column). Numbers for each group are in the bottom of each column. $^*P < 0.05$ (paired *t* test).

$P2Y_1R$ modulation of I_{CAN}. We next addressed whether activation of $P2Y_1R$-mediated signalling pathways potentiates the PIC, and then specifically whether these pathways potentiate the I_{CAN} portion of the PIC. Voltage ramps were applied in control and then again during the local application of MRS2365 that began 10 s prior to the first ramp. MRS2365 significantly potentiated PIC magnitude by 14 ± 4% above control from −131 ± 15 to −152 ± 16 pA (Fig. 10*A*, $n = 12$, $P < 0.05$). This analysis is based on the average of all 12 MNs. MRS2365, however, modulated PIC magnitude in only 8 of these 12 MNs. If these 8 MNs are analysed separately, MRS2365 potentiated PIC magnitude by 21 ± 4% (−117.6 ± 0.9 to −150.7 ± 1.0 pA, $n = 8$, $P < 0.05$, paired *t* test). MRS2365 had no effect on input resistance (177 ± 17 MΩ in control *vs.* 174 ± 16 MΩ in MRS2365, $P > 0.05$). In a separate series of control experiments, local application of aCSF was associated with an insignificant 5 ± 7% change in PIC amplitude ($n = 7$, $P > 0.05$, paired *t* test).

To determine whether $P2Y_1R$ activation potentiates I_{CAN} specifically, we tested whether the $P2Y_1R$-mediated PIC potentiation was sensitive to FFA. After the control voltage ramps, FFA was locally applied for 2.5 min and additional voltage ramps applied to assess the PIC in FFA. MRS2365 was then applied locally for 15 s (in the continued presence of FFA) prior to a final series of voltage ramps to assess the PIC in MRS2365/FFA. As described above, bath-application of FFA caused a significant, 40 ± 11%, decrease in PIC magnitude (Fig. 10*B*, $P < 0.05$). Unlike its potentiating actions in control, MRS2365 had no effect on PIC magnitude in the presence of FFA (−99 ± 25 pA in FFA *vs.* −88 ± 27 pA in MRS2365 and FFA, Fig. 10*B*, $P > 0.05$). Input resistance increased 11 ± 3% from control to FFA (169 ± 34 *vs.* 186 ± 38 MΩ, $P < 0.05$), but there was no effect of MRS2365 on input resistance (186 ± 38 *vs.* 194 ± 37 MΩ, $P > 0.05$).

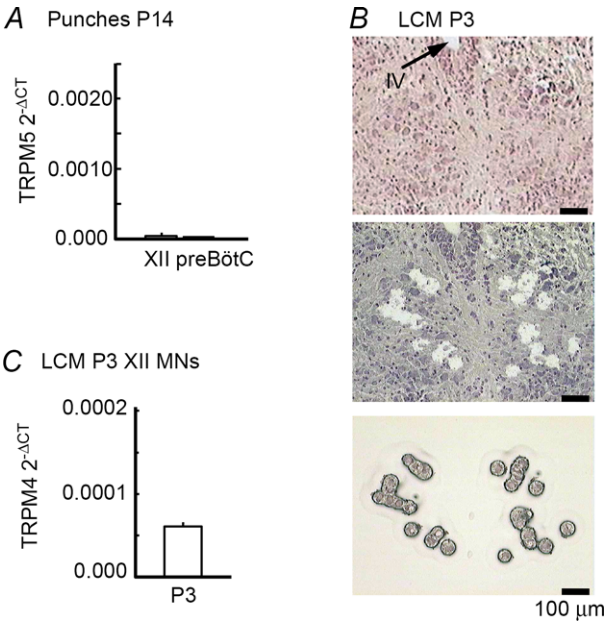

Figure 9. XII MNs express the transcript for TRPM4
A, mRNA extracted from XII and preBötC tissue punches was subject to real-time PCR analysis for the TRPM5 transcripts. Expression levels are reported relative to *cyclophilin A* (ΔCT = cycle threshold number for TRPM*x* – cycle threshold number for *cyclophilin A*). *B*, phototriad showing the XII nucleus in a stained tissue section (6 µm) before and after laser-capture microdissection (LCM; Arcturus AutoPIX II) of XII MNs. The image at the bottom is of captured neurons. *C*, mRNA extracted from laser-captured XII MNs of P3 rats was subject to real-time PCR analysis for the TRPM4 transcripts. Expression levels are reported as described above.

Finally, we obtained whole-cell recordings from inspiratory-modulated XII MNs, identified by the presence of rhythmic inward drive currents in phase with bursts of inspiratory-related activity recorded from the XII nerve. We then bath-applied TTX (0.5 µM) to focus on postsynaptic mechanisms. To test whether $P2Y_1R$ activation potentiates postsynaptic glutamate currents, we measured the current responses from a holding potential of –60 mV evoked by brief puffs of glutamate (500 ms, 100 µM) during the last 30 s of a 2 min local application of aCSF (control) and then during the last 30 s of a 2 min MRS2365 application. Fifteen minutes later, glutamate puffs were reapplied during the last 30 s of a coapplication of MRS2365 and FFA. Local application of 1 mM MRS2365 potentiated glutamate current amplitude by 27 ± 7% from −160 ± 29 pA to −207 ± 44 pA ($n = 7$) (Fig. 11*A*, left panel; and *B*, $P < 0.05$). After washout of MRS2365 (15 min), the glutamate currents returned toward control (−176 ± 55 pA; $n = 5$). In the presence of FFA (100 µM), MRS2365 was associated with an insignificant 4 ± 5% change in glutamate current amplitude (−154 ± 30 pA in control and −163 ± 38 pA in MRS2365 and FFA, $P > 0.05$) (Fig. 11*A*, right panel; and *B*). These data suggest in XII MNs that postsynaptic responses to exogenous glutamate are amplified by a $P2Y_1R$-mediated potentiation of an FFA-sensitive PIC such as I_{CAN}. An important caveat is that even though these experiments were performed in voltage-clamp at a holding potential of –60 mV, the data do not indicate that I_{CAN} was activated solely by a $P2Y_1R$-mediated, intracellular store-derived increase in intracellular Ca^{2+}. Both depolarization and increased intracellular Ca^{2+} are required to activate I_{CAN} (Ullrich *et al.* 2005). Given the morphological complexity of XII MNs, voltage control of the dendrites is unlikely (Spruston *et al.* 1993). I_{CAN} activation during glutamate application therefore most likely reflects glutamate-mediated depolarization of unclamped regions of the dendritic tree and increases in intracellular Ca^{2+} that derive either via activation of voltage-activated Ca^{2+} channels on unclamped membrane or $P2Y_1R$-evoked release of Ca^{2+} from intracellular stores.

Discussion

The significance of P2R signalling in controlling motor output from the brain is poorly understood. Our previous work *in vitro* has demonstrated that local application of ATP over XII MNs innervating airway muscles (Funk *et al.* 1997), and phrenic MNs innervating the major inspiratory pump muscle (Miles *et al.* 2002) causes a biphasic response comprising an initial P2R-mediated excitatory phase, during which both tonic discharge and inspiratory burst amplitude increase, followed by an inhibitory phase when inspiratory burst amplitude decreases. The inhibitory phase is due, at least in part, to the hydrolysis of ATP by ectonucleotidases into adenosine and the inhibitory actions of adenosine at P1Rs (Funk *et al.* 1997; Miles *et al.* 2002). The initial excitatory response was primarily attributed to a P2XR mechanism (Funk *et al.* 1997; Kanjhan *et al.* 1999; Miles *et al.* 2002; Gourine *et al.* 2003). However, in this study we use brainstem–spinal cord and rhythmically active medullary slice preparations to show the following. (i) Activation of P2YRs, especially $P2Y_1Rs$, evokes tonic discharge from XII and C4 ventral nerve roots and potentiates population inspiratory motor output from XII and phrenic MN pools. (ii) The activity of the XII MN pool is at least 10-fold more sensitive to $P2Y_1R$ modulation than the C4 pool of phrenic MNs. (iii) $P2Y_1R$ activation enhances non-inspiratory as well as glutamatergic, inspiratory synaptic activity. (iv) In XII MNs, the $P2Y_1R$-mediated potentiation of inspiratory activity appears to occur indirectly through potentiation of I_{CAN} in a majority of XII MNs, which in turn amplifies glutamatergic synaptic inputs. Indeed, the TRPM4 transcript, which is believed to mediate I_{CAN}, is present in XII MNs. Thus, the excitatory actions of ATP on MN excitability will reflect the combined actions of a postsynaptic, P2XR-dependent inward current that causes membrane depolarization, and a $P2Y_1R$-mediated potentiation of I_{CAN}.

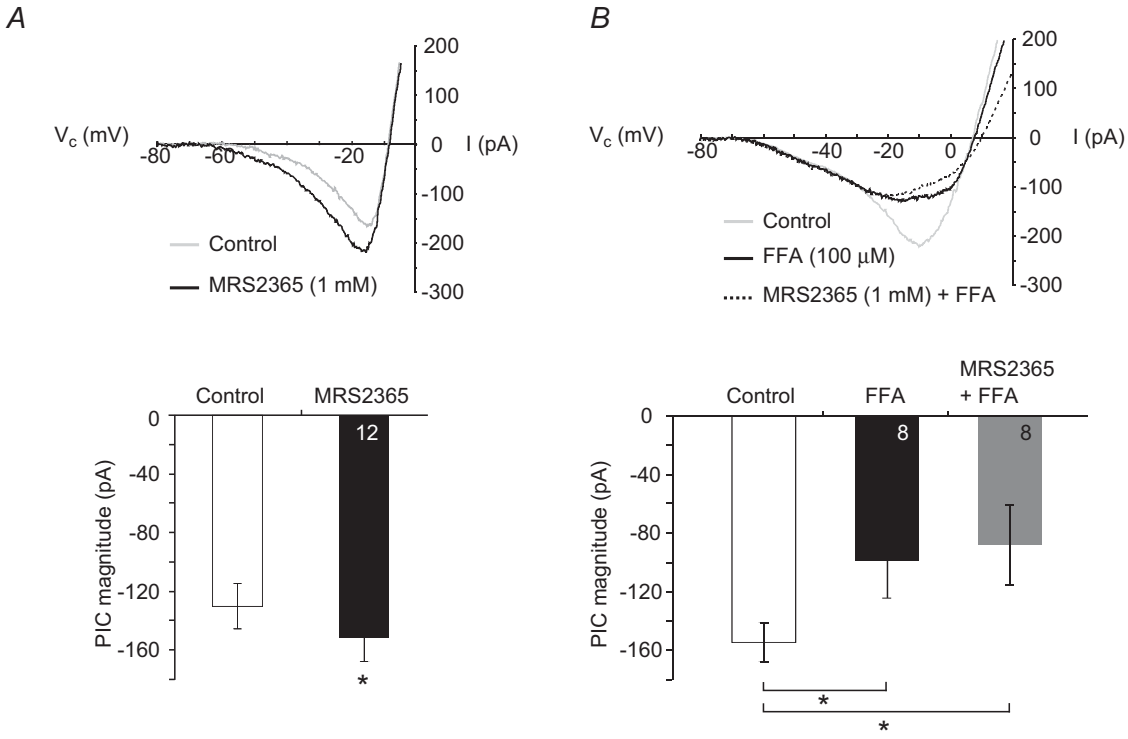

Figure 10. $P2Y_1R$ activation potentiates the XII MN PIC through an FFA-sensitive mechanism
A, top: leak-subtracted (filtered) current response showing PIC evoked by slow voltage-ramp in control and during local application of MRS2365 (1 mM), in TTX. Bottom: group data showing peak PIC amplitude evoked during control (open) and after local application of MRS2365 (1 mM, 15 s, black column; $n = 12$. $^*P < 0.05$, two-tailed paired *t* test. *B*, pre-application of 100 μM FFA prevents MRS2365 potentiation of PIC magnitude (in TTX). Top panel: leak-subtracted (filtered) current response showing PIC evoked by slow voltage-ramp in control, after local application of FFA (black line), or after local application of MRS2365 and FFA (dashed black line). Bottom panel: group data showing peak PIC amplitude evoked in control (open), after 2.5 min of locally applied FFA (2.5 min, black column) and after MRS 2365 (1 mM, 15 s) applied at the end of a 2.5 min application of FFA (grey column). $^*P < 0.05$ (*post hoc* analysis, Newman–Keuls multiple comparison test).

Mechanisms underlying the P2YR-mediated modulation of inspiratory root activity

Receptor subtypes. The increase in tonic discharge and potentiation of inspiratory burst amplitude evoked here by P2YR agonists 2MeSADP and MRS2365 are also features of the response evoked by ATP. These effects were initially attributed to P2XRs based on: (i) immunohistochemical and molecular evidence for these receptors on the MNs; (ii) antagonism of the ATP excitation by low concentrations of the P2R antagonist PPADS; and (iii) the observation that in synaptically isolated MNs, ATP evokes postsynaptic inward currents that are associated with increased conductance suggesting a directly-gated ion channel (Funk *et al.* 1997; Miles *et al.* 2002). Several observations support a P2YR-specific effect as well. First, 2MeSADP and MRS2365 have very low affinities for P2XRs (Chhatriwala *et al.* 2004; Carrasquero *et al.* 2005; León *et al.* 2006; Kahlert *et al.* 2007; Ortega *et al.* 2008). Second, the cellular effects of ATP and 2MeSADP/MRS2365 on XII MN properties are distinct. Whereas ATP evokes a postsynaptic current in synaptically isolated XII MNs by opening an ion channel (Funk *et al.* 1997), 2MeSADP and MRS2365 had no effect on synaptically isolated XII MNs held at resting potential. A postsynaptic effect was only detected when the membrane was depolarized to reveal a PIC that was potentiated by MRS2365. Third, as confirmed here, XII MNs show immunolabelling for $P2Y_1$Rs (Fong *et al.* 2002; and present results). Whether XII MNs are sensitive only to $P2Y_1$ or to other P2YRs is not clear. The fact that the selective $P2Y_1$ agonist MRS2365, and the more general P2YR agonist 2MeSADP, produced similar effects on XII burst amplitude suggests that $P2Y_1$Rs are the main contributor, but a role for other receptor P2YR subtypes cannot be excluded.

The relative potencies of P2Y *vs.* P2XR mechanisms were not compared. Exogenous ATP applied to the XII nucleus of rhythmic slices potentiates XII inspiratory burst amplitude by 40 ± 20% (Funk *et al.* 1997), similar to that evoked here by $P2Y_1$R agonists. Given that ATP activates both P2X and P2YRs, one would predict a greater effect of ATP. However, it is possible that rapid degradation of ATP by ectonucleotidases will result in submaximal effects compared to the P2YR agonists used here (2MeSADP and MRS2365). These two agonists are substrates for ectonucleoside triphosphate diphosphohydrolases (E-NTPDases), but the monophosphate derivatives are not broken down to adenosine (Ravi *et al.* 2002; Alvarado-Castillo *et al.* 2005; Robson *et al.* 2006). Assessing the relative contribution of P2X and P2Y receptors to the effects of ATP was not our objective and will require assessing the actions of ATP before and during application of selective P2X and P2Y receptor antagonists.

Cellular and synaptic mechanisms. Our mechanistic studies focused on analysis of XII MNs because the high concentration of agonist required to potentiate C4 output raised questions of physiological relevance. At least three mechanisms could contribute to the P2YR-mediated

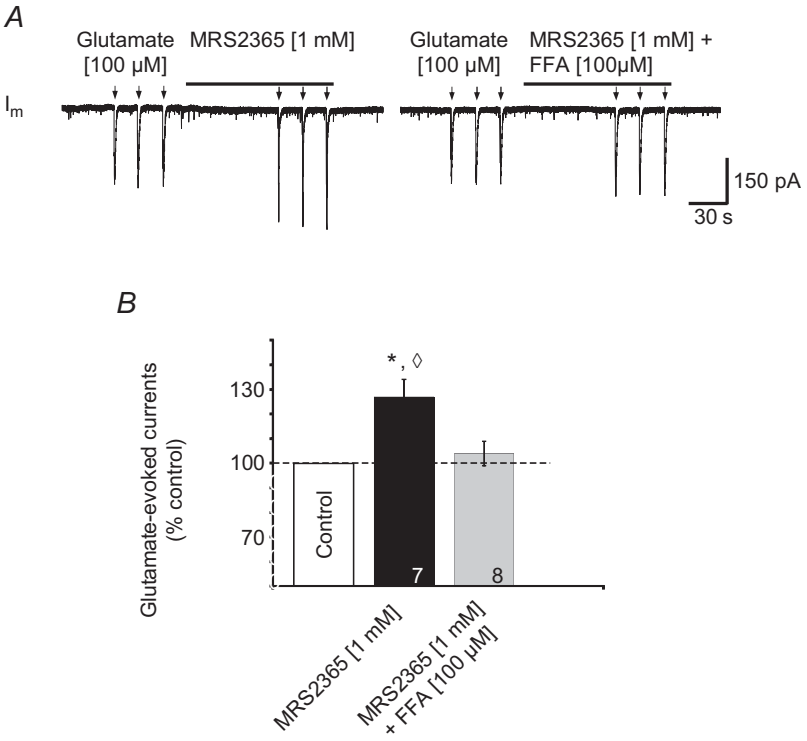

Figure 11. $P2Y_1$R activation potentiates glutamate currents through an FFA-sensitive mechanism
A, voltage-clamp recording of a XII MN held at –60 mV illustrating currents evoked by glutamate puffs (100 μM, 500 ms) in control and in the presence of MRS2365 (left trace), and then again in the presence of MRS2365 and 100 μM FFA (right trace). *B*, group data showing, relative to control, the change in peak glutamate currents evoked by local application of MRS2365 alone or in combination with FFA. Numbers for each group are in the bottom of each column; * indicates significant difference from control; ◊ indicates significant difference to MRS2365 (1 mM) + FFA (100 μM); $P < 0.05$ (*post hoc* analysis, Bonferroni method).

activation of tonic discharge and potentiation of XII (and possibly C4) inspiratory burst amplitude. (i) P2YRs could directly depolarize MNs via modulation of a conductance active at rest, as seen in hippocampal neurons and in *Xenopus* embryos (Brown & Dale, 2002) where P2YRs block an M-type potassium current (Filippov *et al.* 2006). Our initial observation that 2MeSADP and MRS2365 evoke small inward currents suggested activation of postsynaptic receptors and direct depolarization. However, the virtual loss of these currents upon bath application of TTX indicates that these actions are unlikely to be due to activation of postsynaptic receptors that modify a current active at rest. (ii) P2YR-mediated potentiation of glutamatergic inspiratory synaptic currents through pre- or postsynaptic mechanisms, as observed in rat medial habenula (Price *et al.* 2003) and nucleus accumbens (Krügel *et al.* 2004) where P2YR activation potentiates presynaptic glutamate release, could also contribute. The increase in the frequency of EPSCs and amplitude of inspiratory currents following agonist application suggested both pre- and postsynaptic potentiation of glutamatergic transmission. Loss of these effects in TTX, however, indicates that they were not via direct modulation of glutamatergic transmission. (iii) P2YR activation could also increase MN excitability through modulation of a conductance not active at rest such that a greater output would be produced for the same synaptic input. We hypothesized that the P2YR potentiation of inspiratory activity is due to the potentiation of a Ca^{2+}-activated, non-selective cation current, which then potentiates synaptic inputs. This hypothesis was based on the demonstration in preBötC neurons that metabotropic glutamate receptor (mGluR) activation evokes such a mechanism (Pace *et al.* 2007), and that mGluRs and $P2Y_1$Rs both signal through phospholipase C which can potentiate I_{CAN} (Simon *et al.* 1995; von Kugelgen & Wetter, 2000; Sak & Illes, 2005; Crowder *et al.* 2007; Pace *et al.* 2007; Guinamard *et al.* 2011). Several lines of evidence support this hypothesis. First, PCR analysis of XII punches and laser-captured XII MNs revealed the transcript for TRPM4 but very little TRPM5, which is consistent with the limited CNS expression of TRPM5 compared to TRPM4 (Guinamard *et al.* 2011). TRPM4 and TRPM5 are most commonly considered candidates for I_{CAN} (Guinamard *et al.* 2011), although a recent paper presented evidence that TRPV2 may be a major contributor to I_{CAN} in spinal MNs (Bouhadfane *et al.* 2013). However, the fact that the TRPV2 is virtually inactive at the temperatures used in these experiments (Caterina *et al.* 1997) combined with our demonstration that the TRPM4 blocker 9-phenanthrol attenuates the Ca^{2+}-mediated PIC by ∼33%, indicate that TRPM4 is a significant contributor to I_{CAN} in XII MNs.

Second, sensitivity of the PIC to FFA, high BAPTA and 9-phenanthrol provide electrophysiological and pharmacological evidence that I_{CAN} contributes to the PIC in XII MNs. I_{CAN} is a component of plateau potentials in turtle MNs (Perrier & Hounsgaard, 1999), and PICs in rostral ambigual (Rekling & Feldman, 1997) and dorsal gastric MNs (Zhang *et al.* 1995). I_{CAN} also contributes to long-lasting excitatory currents in deep dorsal horn neurons (Morisset & Nagy, 1999), locomotor-related spinal interneurons (Dai & Jordan, 2010), and preBötC inspiratory neurons (Pace *et al.* 2007). In XII MNs, the PIC is primarily attributed to an equal contribution from voltage-gated Ca^{2+} currents and persistent sodium current (I_{NaP}) (Powers & Binder, 2003). A contribution of I_{CAN} to the PIC was proposed in neonatal rat (Lamanauskas & Nistri, 2008), but this possibility was rejected based on analysis of juvenile XII MNs in which substitution of Na^+ (a major charge carrier of I_{CAN}) had minimal effect on the PIC (Powers & Binder, 2003). In contrast, our data in neonates showing that FFA reduces the PIC by ∼15% (Fig. 8*B*) suggest that I_{CAN} contributes a small but significant portion of the total XII MN PIC. Consistent with this, when the Ca^{2+}-dependent component of the PIC was isolated using TTX to exclude I_{NaP}, the FFA-sensitive component (presumptive I_{CAN}) contributed ∼40%. In addition, in TTX using high intracellular BAPTA solution, which will block Ca^{2+}-dependent currents like I_{CAN} but not voltage-gated Ca^{2+} currents, the PIC was reduced by 47%, suggesting that I_{CAN} contributes significantly to the TTX-resistant PIC. Finally, the 33% inhibition of the PIC by 9-phenanthrol, which blocks a TRPM4-mediated I_{CAN}, further supports the conclusion that the XII MN PIC includes an I_{CAN} component.

There are two important caveats regarding the use of FFA to measure I_{CAN}. First, at the concentration of 100 μM used here, FFA does not completely block I_{CAN} (Guinamard *et al.* 2013). Thus, our measurements with FFA may underestimate the contribution of I_{CAN} to XII MN PICs. Second, sensitivity to 100 μM is not definitive evidence of I_{CAN}. FFA is an aromatic amino acid with a broad spectrum of ion channel targets. Its highest affinity is for non-selective cation channels including TRPM4 and TRPM5. FFA concentration was limited to 100 μM to minimize off-target actions. However, even at 100 μM FFA actions on chloride channels, Ca^{2+}-activated K^+ channels, some two-pore domain K^+ channels, and L-type Ca^{2+} channels, cannot be excluded (Shimamura *et al.* 2002; Guinamard *et al.* 2013). Nevertheless, off-target actions in our experiments were unlikely. The actual concentration of FFA experienced by the XII MNs in our experiments was more likely to be in the range of 10 μM because FFA was locally applied rather than bath-applied. Drug concentration falls off exponentially from a point source and previous work with this preparation indicates that the pipette concentration must be ∼10-fold higher than the bath concentration to produce similar effects (Liu *et al.* 1990). Our electrophysiology data further support

the selective action of FFA on I_{CAN}. Had FFA activated Ca^{2+}-activated or two-pore domain K^+ channels, MN input resistance should have decreased. FFA either had no effect on input resistance or caused a slight increase.

BAPTA sensitivity of the PIC potentiation also does not definitively establish I_{CAN} involvement. BAPTA will not affect voltage-gated Ca^{2+} channels. However, in turtle lumbar MNs BAPTA blocks an I_{CAN}-independent, Ca^{2+}- and calmodulin-dependent PIC potentiation (Perrier *et al.* 2000). Whether a similar pathway exists in mammalian MNs is not known. If it does, our measurements based on BAPTA sensitivity may overestimate the contribution of I_{CAN} to the XII MN PIC. The fact that FFA and high BAPTA caused similar reductions in the TTX-insensitive PIC, however, suggests that over-estimation is unlikely and therefore that I_{CAN} contributes 40–47% of the Ca^{2+}-dependent PIC in our experiments. Based on estimates that I_{NaP} and the Ca^{2+} component each form ∼50% of the total PIC (Powers & Binder, 2003), the I_{CAN} component probably forms 20–25% of the total PIC in XII MNs. This is smaller than its contribution in deep dorsal horn interneurons (Morisset & Nagy, 1999), but larger than in locomotor-related spinal interneurons (Dai & Jordan, 2010). Whether TRPM4 underlies all of the I_{CAN} in XII MNs is not clear. The fact that the 9-phenanthrol block of the PIC in TTX was only 33% while it was 40% and 47% in FFA and high BAPTA suggests that it may not be exclusively TRPM4.

The second piece of evidence supporting our hypothesis that the $P2Y_1R$ potentiation of inspiratory activity is via potentiation of I_{CAN} is that MRS2365 significantly potentiated the XII MN PIC by 21% and that this potentiation was completely blocked by FFA. At the very least these data indicate that MRS2365 is acting via an FFA-sensitive PIC.

The third body of evidence supporting our hypothesized mechanism is that the $P2Y_1R$-mediated potentiation of glutamatergic signalling appears dependent on I_{CAN}. In identified inspiratory neurons synaptically isolated in TTX, MRS2365 potentiation of glutamate-evoked currents was blocked by FFA. Taken together, these data provide strong evidence that $P2Y_1R$ signalling potentiates glutamatergic inputs to XII MNs, at least in part through the potentiation of an FFA- and BAPTA-sensitive PIC that is most likely the non-selective cation current I_{CAN}.

Physiological significance of P2YR signalling in modulating inspiratory MN activity

In phrenic and XII nuclei, exogenous ATP evokes a biphasic response comprising an initial, rapid, P2R-mediated excitation followed by a P1R-mediated inhibition (Funk *et al.* 1997; Miles *et al.* 2002). Data presented here suggest that $P2Y_1Rs$ will contribute to the initial excitatory phase, and possibly offset the magnitude of the secondary inhibition.

Understanding the true physiological significance requires more information about the conditions or stimuli that evoke the release of endogenous ATP. At present, virtually nothing is known of the stimuli that evoke ATP release onto inspiratory MNs in mammals. In *Xenopus* tadpole, ATP is released in response to tail pinch where it acts via a P2YR-like excitatory process to initiate swimming and a competing adenosinergic inhibitory mechanism to terminate rhythmic activity (Dale & Gilday, 1996). In anaesthetized rats, different compartments of the ventral respiratory network appear to release ATP in response to hypercapnia or hypoxia (Gourine *et al.* 2005*a*,*b*), which in turn may contribute to the respective homeostatic ventilatory responses. Hypercapnia appears to evoke ATP release from astrocytes in the retotrapezoid nucleus, where it excites chemosensitive Phox2b neurons, enhances their excitability and contributes as much as 20% to the ventilatory response (Gourine *et al.* 2005*b*). Also in anaesthetized adult rats, hypoxia appears to evoke ATP release from the ventral respiratory group, where it attenuates the secondary hypoxic ventilatory depression (Gourine *et al.* 2005*b*), perhaps through $P2Y_1Rs$ in the preBötC (Lorier *et al.* 2007). CO_2 or hypoxia-induced release of ATP in motor nuclei would probably increase MN excitability and tidal volume, either by increasing activity of the pump muscles or decreasing airway resistance through increased activity of airway dilator muscles, like those innervated by XII MNs. Of these two possibilities, a reduction in airway resistance is most likely given that XII MNs appear >10 times more sensitive to P2YR modulation than phrenic MNs. The sensitivity of XII MNs to ATP (Funk *et al.* 1997) was similarly reported as ∼10-fold greater than that of phrenic MNs (Miles *et al.* 2002). However, direct comparison between these earlier studies was difficult due to potential differences in antagonist access to the two MN pools. Our demonstration that GABA caused equivalent inhibition of XII and C4 inspiratory output suggests equal drug access to both nuclei and therefore greater sensitivity of XII MNs to P2YR activation. In fact the high concentration of P2YR agonists required to potentiate C4 inspiratory nerve output suggests that P2YR signalling has minimal physiological significance in modulating phrenic MN excitability. Spinal MNs do not appear to express $P2Y_1Rs$ (Kobayashi *et al.* 2006), but they do express $P2Y_4$ and $P2Y_6Rs$. A role for P2YRs cannot be excluded, however, because phrenic MNs have not been examined specifically. In addition, $P2Y_1Rs$ activate a non-specific cation current in lamina IX neurons, some of which may be MNs (Aoyama *et al.* 2010).

The source of ATP will also be a critical factor determining the physiological effects of endogenously released ATP, as ATP is often a cotransmitter that

has multiple linear and non-linear interactions with other transmitters (Richardson & Brown, 1987; Funk *et al.* 1997; Matsuka *et al.* 2001; Mori *et al.* 2001; Jo & Role, 2002). The potential co-release of ATP with noradrenaline is perhaps most relevant in the context of the differential sensitivity of XII and phrenic MNs to ATP and sleep-disordered breathing. Compared to pump MNs (phrenic), the greater susceptibility of airway MNs (XII) to sleep-related reductions in tone through disfacilitation (loss of excitatory modulatory inputs during sleep) is a hypothesized factor in sleep-disordered breathing (Chan *et al.* 2006; Horner, 2008, 2011). Locus coeruleus (LC) neurons co-release ATP with noradrenaline (Poelchen *et al.* 2001). Their activity is state dependent (Aston-Jones & Bloom, 1981), i.e. they are active in wakefulness but virtually silent during rapid-eye-movement (REM) sleep. Thus, loss of noradrenaline and ATP inputs during REM sleep could reduce excitability. LC neurons provide only a small portion of the noradrenergic input to XII MNs. However, if noradrenergic neurons innervating the XII nucleus also co-release ATP and show state-dependent reductions in activity, loss of noradrenaline and purinergic tone could contribute to the greater susceptibility of airway MNs to atonia in REM.

Another potential source of ATP is from glial cells. Evidence obtained *in vitro* and *in vivo* suggest that glia on the ventral surface of the medulla at the retrotrapezoid nucleus release ATP in response to acidic pH (Gourine *et al.* 2010) or elevated CO_2 (Huckstepp *et al.* 2010*a*,*b*; Meigh *et al.* 2013) and that the ATP excites chemosensitive RTN neurons, thereby contributing to central chemosensitivity (Gourine *et al.* 2010; Huckstepp *et al.* 2010*a*,*b*; Sobrinho *et al.* 2014). Whether glial cells in motor nuclei respond to hypoxia or other stimuli by releasing ATP is not known but it is possible. In the carotid body, ATP is released from Type-1 glomus cells in hypoxia and this is hypothesized to evoke ATP release from glial-like, type II sustentacular cells (Nurse & Piskuric, 2013). Within the CNS, hippocampal astrocytes release adenosine in response to hypoxia (Martin *et al.* 2007), while spontaneous Ca^{2+} waves in cerebellar Bergmann glia increase in hypoxia (Mathiesen *et al.* 2013).

In summary, our data indicate in mammals that the inspiratory output of XII MNs that control the airway is sensitive to modulation by $P2Y_1$Rs, at least in part via potentiation of an I_{CAN} current that amplifies glutamatergic inputs and is most likely mediated by TRPM4.

References

Abbracchio MP, Burnstock G, Verkhratsky A & Zimmermann H (2009). Purinergic signalling in the nervous system: an overview. *Trends Neurosci* **32**, 19–29.

Adachi T, Huxtable AG, Fang X & Funk GD (2010). Substance P modulation of hypoglossal motoneuron excitability during development: changing balance between conductances. *J Neurophysiol* **104**, 854–872.

Adachi T, Robinson DM, Miles GB & Funk GD (2005). Noradrenergic modulation of XII motoneuron inspiratory activity does not involve α_2-receptor inhibition of the I_h current or presynaptic glutamate release. *J Appl Physiol* **98**, 1297–1308.

Alvarado-Castillo C, Harden TK & Boyer JL (2005). Regulation of $P2Y_1$ receptor-mediated signaling by the ectonucleoside triphosphate diphosphohydrolase isozymes NTPDase1 and NTPDase2. *Mol Pharmacol* **67**, 114–122.

Aoyama T, Koga S, Nakatsuka T, Fujita T, Goto M & Kumamoto E (2010). Excitation of rat spinal ventral horn neurons by purinergic P2X and P2Y receptor activation. *Brain Res* **1340**, 10–17.

Aston-Jones G & Bloom FE (1981). Activity of norepinephrine-containing locus coeruleus neurons in behaving rats anticipates fluctuations in the sleep-waking cycle. *J Neurosci* **1**, 876–886.

Bellingham MC (2013). Pre- and postsynaptic mechanisms underlying inhibition of hypoglossal motor neuron excitability by riluzole. *J Neurophysiol* **110**, 1047–1061.

Bouhadfane M, Tazerart S, Moqrich A, Vinay L & Brocard F (2013). Sodium-mediated plateau potentials in lumbar motoneurons of neonatal rats. *J Neurosci* **33**, 15626–15641.

Brown P & Dale N (2002). Modulation of K^+ currents in *Xenopus* spinal neurons by P2Y receptors: a role for ATP and ADP in motor pattern generation. *J Physiol* **540**, 843–850.

Burnstock G (2007). Physiology and pathophysiology of purinergic neurotransmission. *Physiol Rev* **87**, 659–797.

Carrasquero LM, Delicado EG, Jiménez AI, Pérez-Sen R & Miras-Portugal MT (2005). Cerebellar astrocytes co-express several ADP receptors. Presence of functional $P2Y_{13}$-like receptors. *Purinergic Signal* **1**, 153–159.

Caterina MJ, Schumacher MA, Tominaga M, Rosen TA, Levine JD & Julius D (1997). The capsaicin receptor: a heat-activated ion channel in the pain pathway. *Nature* **389**, 816–824.

Chan E, Steenland HW, Liu H & Horner RL (2006). Endogenous excitatory drive modulating respiratory muscle activity across sleep-wake states. *Am J Respir Crit Care Med* **174**, 1264–1273.

Chhatriwala M, Ravi RG, Patel RI, Boyer JL, Jacobson KA & Harden TK (2004). Induction of novel agonist selectivity for the ADP-activated $P2Y_1$ receptor versus the ADP-activated $P2Y_{12}$ and $P2Y_{13}$ receptors by conformational constraint of an ADP analog. *J Pharmacol Exp Ther* **311**, 1038–1043.

Collo G, North RA, Kawashima E, Merlo-Pich E, Neidhart S, Surprenant A & Buell G (1996). Cloning OF $P2X_5$ and $P2X_6$ receptors and the distribution and properties of an extended family of ATP-gated ion channels. *J Neurosci* **16**, 2495–2507.

Cramer NP, Li Y & Keller A (2007). The whisking rhythm generator: a novel mammalian network for the generation of movement. *J Neurophysiol* **97**, 2148–2158.

Crowder EA, Saha MS, Pace RW, Zhang H, Prestwich GD & Del Negro CA (2007). Phosphatidylinositol 4,5-bisphosphate regulates inspiratory burst activity in the neonatal mouse preBötzinger complex. *J Physiol* **582**, 1047–1058.

Dai Y & Jordan LM (2010). Multiple patterns and components of persistent inward current with serotonergic modulation in locomotor activity-related neurons in Cfos-EGFP mice. *J Neurophysiol* **103**, 1712–1727.

Dale N & Gilday D (1996). Regulation of rhythmic movements by purinergic neurotransmitters in frog embryos. *Nature* **383**, 259–263.

Enríquez Denton M, Wienecke J, Zhang M, Hultborn H & Kirkwood PA (2012). Voltage-dependent amplification of synaptic inputs in respiratory motoneurones. *J Physiol* **590**, 3067–3090.

Filippov AK, Choi RC, Simon J, Barnard EA & Brown DA (2006). Activation of $P2Y_1$ nucleotide receptors induces inhibition of the M-type K^+ current in rat hippocampal pyramidal neurons. *J Neurosci* **26**, 9340–9348.

Fong AY, Krstew EV, Barden J & Lawrence AJ (2002). Immunoreactive localisation of P2Y1 receptors within the rat and human nodose ganglia and rat brainstem: comparison with [α^{33}P]deoxyadenosine 5′-triphosphate autoradiography. *Neuroscience* **113**, 809–823.

Funk GD, Huxtable AG & Lorier AR (2008). ATP in central respiratory control: a three-part signaling system. *Respir Physiol Neurobiol* **164**, 131–142.

Funk GD, Kanjhan R, Walsh C, Lipski J, Comer AM, Parkis MA & Housley GD (1997). P2 receptor excitation of rodent hypoglossal motoneuron activity *in vitro* and *in vivo*: a molecular physiological analysis. *J Neurosci* **17**, 6325–6337.

Funk GD, Smith JC & Feldman JL (1993). Generation and transmission of respiratory oscillations in medullary slices: role of excitatory amino acids. *J Neurophysiol* **70**, 1497–1515.

Funk GD, Zwicker JD, Selvaratnam R & Robinson DM (2011). Noradrenergic modulation of hypoglossal motoneuron excitability: developmental and putative state-dependent mechanisms. *Arch Ital Biol* **149**, 426–453.

Gourine AV, Atkinson L, Deuchars J & Spyer KM (2003). Purinergic signalling in the medullary mechanisms of respiratory control in the rat: respiratory neurones express the $P2X_2$ receptor subunit. *J Physiol* **552**, 197–211.

Gourine AV, Kasymov V, Marina N, Tang F, Figueiredo MF, Lane S, Teschemacher AG, Spyer KM, Deisseroth K & Kasparov S (2010). Astrocytes control breathing through pH-dependent release of ATP. *Science* **329**, 571–575.

Gourine AV, Llaudet E, Dale N & Spyer KM (2005*a*). ATP is a mediator of chemosensory transduction in the central nervous system. *Nature* **436**, 108–111.

Gourine AV, Llaudet E, Dale N & Spyer KM (2005*b*). Release of ATP in the ventral medulla during hypoxia in rats: role in hypoxic ventilatory response. *J Neurosci* **25**, 1211–1218.

Guinamard R, Salle L & Simard C (2011). The non-selective monovalent cationic channels TRPM4 and TRPM5. *Adv Exp Med Biol* **704**, 147–171.

Guinamard R, Simard C & Del Negro C (2013). Flufenamic acid as an ion channel modulator. *Pharmacol Ther* **138**, 272–284.

Hamm TM, Turkin VV, Bandekar NK, O'Neill D & Jung R (2010). Persistent currents and discharge patterns in rat hindlimb motoneurons. *J Neurophysiol* **104**, 1566–1577.

Hofmann T, Chubanov V, Gudermann T & Montell C (2003). TRPM5 is a voltage-modulated and Ca^{2+}-activated monovalent selective cation channel. *Curr Biol* **13**, 1153–1158.

Horner RL (2008). Neuromodulation of hypoglossal motoneurons during sleep. *Resp Physiol Neurobiol* **164**, 179–196.

Horner RL (2011). The tongue and its control by sleep state-dependent modulators. *Arch Ital Biol* **149**, 406–425.

Hounsgaard J, Hultborn H, Jespersen B & Kiehn O (1988). Bistability of α-motoneurones in the decerebrate cat and in the acute spinal cat after intravenous 5-hydroxytryptophan. *J Physiol* **405**, 345–367.

Hounsgaard J & Kiehn O (1989). Serotonin-induced bistability of turtle motoneurones caused by a nifedipine-sensitive calcium plateau potential. *J Physiol* **414**, 265–282.

Hsiao CF, Del Negro CA, Trueblood PR & Chandler SH (1998). Ionic basis for serotonin-induced bistable membrane properties in guinea pig trigeminal motoneurons. *J Neurophysiol* **79**, 2847–2856.

Hsiao CF, Trueblood PR, Levine MS & Chandler SH (1997). Multiple effects of serotonin on membrane properties of trigeminal motoneurons in vitro. *J Neurophysiol* **77**, 2910–2924.

Huckstepp RT, Eason R, Sachdev A & Dale N (2010*a*). CO_2-dependent opening of connexin 26 and related β connexins. *J Physiol* **588**, 3921–3931.

Huckstepp RT, id Bihi R, Eason R, Spyer KM, Dicke N, Willecke K, Marina N, Gourine AV & Dale N (2010*b*). Connexin hemichannel-mediated CO_2-dependent release of ATP in the medulla oblongata contributes to central respiratory chemosensitivity. *J Physiol* **588**, 3901–3920.

Hudgel DW & Harasick T (1990). Fluctuation in timing of upper airway and chest wall inspiratory muscle activity in obstructive sleep apnea. *J Appl Physiol (1985)* **69**, 443–450.

Hultborn H & Kiehn O (1992). Neuromodulation of vertebrate motor neuron membrane properties. *Curr Opin Neurobiol* **2**, 770–775.

Huxtable AG, Zwicker JD, Alvares TS, Ruangkittisakul A, Fang X, Hahn LB, Posse de Chaves E, Baker GB, Ballanyi K & Funk GD (2010). Glia contribute to the purinergic modulation of inspiratory rhythm-generating networks. *J Neurosci* **30**, 3947–3958.

Huxtable AG, Zwicker JD, Poon BY, Pagliardini S, Vrouwe SQ, Greer JJ & Funk GD (2009). Tripartite purinergic modulation of central respiratory networks during perinatal development: the influence of ATP, ectonucleotidases, and ATP metabolites. *J Neurosci* **29**, 14713–14725.

Illes P & Alexandre Ribeiro J (2004). Molecular physiology of P2 receptors in the central nervous system. *Eur J Pharmacol* **483**, 5–17.

Illes P & Ribeiro JA (2004). Neuronal P2 receptors of the central nervous system. *Curr Top Med Chem* **4**, 831–838.

Ireland MF, Noakes PG & Bellingham MC (2004). P2X7-like receptor subunits enhance excitatory synaptic transmission at central synapses by presynaptic mechanisms. *Neuroscience* **128**, 269–280.

Jacobson KA, Costanzi S, Joshi BV, Besada P, Shin DH, Ko H, Ivanov AA & Mamedova L (2006). Agonists and antagonists for P2 receptors. *Novartis Found Symp* **276**, 58–68; discussion 68–72, 107–112, 275–181.

Jo YH & Role LW (2002). Coordinate release of ATP and GABA at *in vitro* synapses of lateral hypothalamic neurons. *J Neurosci* **22**, 4794–4804.

Kahlert S, Blaser T, Tulapurkar M & Reiser G (2007). P2Y receptor-activating nucleotides modulate cellular reactive oxygen species production in dissociated hippocampal astrocytes and neurons in culture independent of parallel cytosolic Ca^{2+} rise and change in mitochondrial potential. *J Neurosci Res* **85**, 3443–3456.

Kanjhan R, Housley GD, Burton LD, Christie DL, Kippenberger A, Thorne PR, Luo L & Ryan AF (1999). Distribution of the $P2X_2$ receptor subunit of the ATP-gated ion channels in the rat central nervous system. *J Comp Neurol* **407**, 11–32.

Kobayashi K, Fukuoka T, Yamanaka H, Dai Y, Obata K, Tokunaga A & Noguchi K (2006). Neurons and glial cells differentially express P2Y receptor mRNAs in the rat dorsal root ganglion and spinal cord. *J Comp Neurol* **498**, 443–454.

Koizumi H, Wilson CG, Wong S, Yamanishi T, Koshiya N & Smith JC (2008). Functional imaging, spatial reconstruction, and biophysical analysis of a respiratory motor circuit isolated *in vitro*. *J Neurosci* **28**, 2353–2365.

Krügel U, Schraft T, Regenthal R, Illes P & Kittner H (2004). Purinergic modulation of extracellular glutamate levels in the nucleus accumbens in vivo. *Int J Dev Neurosci* **22**, 565–570.

Lamanauskas N & Nistri A (2008). Riluzole blocks persistent Na^+ and Ca^{2+} currents and modulates release of glutamate via presynaptic NMDA receptors on neonatal rat hypoglossal motoneurons in vitro. *Eur J Neurosci* **27**, 2501–2514.

Lancaster B & Batchelor AM (2000). Novel action of BAPTA series chelators on intrinsic K^+ currents in rat hippocampal neurones. *J Physiol* **522**, 231–246.

Launay P, Fleig A, Perraud AL, Scharenberg AM, Penner R & Kinet JP (2002). TRPM4 is a Ca^{2+}-activated nonselective cation channel mediating cell membrane depolarization. *Cell* **109**, 397–407.

Lee RH & Heckman CJ (2001). Essential role of a fast persistent inward current in action potential initiation and control of rhythmic firing. *J Neurophysiol* **85**, 472–475.

León D, Hervás C & Miras-Portugal MT (2006). $P2Y_1$ and $P2X_7$ receptors induce calcium/calmodulin-dependent protein kinase II phosphorylation in cerebellar granule neurons. *Eur J Neurosci* **23**, 2999–3013.

Li Y & Bennett DJ (2003). Persistent sodium and calcium currents cause plateau potentials in motoneurons of chronic spinal rats. *J Neurophysiol* **90**, 857–869.

Liu G, Feldman JL & Smith JC (1990). Excitatory amino acid-mediated transmission of inspiratory drive to phrenic motoneurons. *J Neurophysiol* **64**, 423–436.

Lorier AR, Huxtable AG, Robinson DM, Lipski J, Housley GD & Funk GD (2007). $P2Y_1$ receptor modulation of the pre-Bötzinger complex inspiratory rhythm generating network *in vitro*. *J Neurosci* **27**, 993–1005.

Lorier AR, Lipski J, Housley GD, Greer JJ & Funk GD (2008). ATP sensitivity of preBötzinger complex neurones in neonatal rat *in vitro*: mechanism underlying a P2 receptor-mediated increase in inspiratory frequency. *J Physiol* **586**, 1429–1446.

Lorier AR, Peebles K, Brosenitsch T, Robinson DM, Housley GD & Funk GD (2004). P2 receptors modulate respiratory rhythm but do not contribute to central CO_2 sensitivity in vitro. *Respir Physiol Neurobiol* **142**, 27–42.

Marchetti C, Pagnotta S, Donato R & Nistri A (2002). Inhibition of spinal or hypoglossal motoneurons of the newborn rat by glycine or GABA. *Eur J Neurosci* **15**, 975–983.

Martin ED, Fernandez M, Perea G, Pascual O, Haydon PG, Araque A & Cena V (2007). Adenosine released by astrocytes contributes to hypoxia-induced modulation of synaptic transmission. *Glia* **55**, 36–45.

Mathiesen C, Brazhe A, Thomsen K & Lauritzen M (2013). Spontaneous calcium waves in Bergman glia increase with age and hypoxia and may reduce tissue oxygen. *J Cereb Blood Flow Metab* **33**, 161–169.

Matsuka Y, Neubert JK, Maidment NT & Spigelman I (2001). Concurrent release of ATP and substance P within guinea pig trigeminal ganglia in vivo. *Brain Res* **915**, 248–255.

Meigh L, Greenhalgh SA, Rodgers TL, Cann MJ, Roper DI & Dale N (2013). CO_2 directly modulates connexin 26 by formation of carbamate bridges between subunits. *Elife* **2**, e01213.

Miles GB, Parkis MA, Lipski J & Funk GD (2002). Modulation of phrenic motoneuron excitability by ATP: consequences for respiratory-related output in vitro. *J Appl Physiol (1985)* **92**, 1899–1910.

Mironov SL (2008). Metabotropic glutamate receptors activate dendritic calcium waves and TRPM channels which drive rhythmic respiratory patterns in mice. *J Physiol* **586**, 2277–2291.

Mironov SL & Skorova EY (2011). Stimulation of bursting in pre-Botzinger neurons by Epac through calcium release and modulation of TRPM4 and K-ATP channels. *J Neurochem* **117**, 295–308.

Mironov SL (2013). Calmodulin and calmodulin kinase II mediate emergent bursting activity in the brainstem respiratory network (preBotzinger complex). *J Physiol* **591**, 1613–1630.

Montell C (2005). The TRP superfamily of cation channels. *Sci STKE* **2005**, re3.

Mori M, Heuss C, Gahwiler BH & Gerber U (2001). Fast synaptic transmission mediated by P2X receptors in CA3 pyramidal cells of rat hippocampal slice cultures. *J Physiol* **535**, 115–123.

Morisset V & Nagy F (1999). Ionic basis for plateau potentials in deep dorsal horn neurons of the rat spinal cord. *J Neurosci* **19**, 7309–7316.

Mulkey DK, Mistry AM, Guyenet PG & Bayliss DA (2006). Purinergic P2 receptors modulate excitability but do not mediate pH sensitivity of RTN respiratory chemoreceptors. *J Neurosci* **26**, 7230–7233.

Nilius B, Prenen J, Tang J, Wang C, Owsianik G, Janssens A, Voets T & Zhu MX (2005). Regulation of the Ca^{2+} sensitivity of the nonselective cation channel TRPM4. *J Biol Chem* **280**, 6423–6433.

Nolan T, Hands RE & Bustin SA (2006). Quantification of mRNA using real-time RT-PCR. *Nat Protoc* **1**, 1559–1582.

North RA (2002). Molecular physiology of P2X receptors. *Physiol Rev* **82**, 1013–1067.

Núñez-Abades PA & Cameron WE (1995). Morphology of developing rat genioglossal motoneurons studied in vitro: relative changes in diameter and surface area of somata and dendrites. *J Comp Neurol* **353**, 129–142.

Núñez-Abades PA, He F, Barrionuevo G & Cameron WE (1994). Morphology of developing rat genioglossal motoneurons studied in vitro: changes in length, branching pattern, and spatial distribution of dendrites. *J Comp Neurol* **339**, 401–420.

Nurse CA & Piskuric NA (2013). Signal processing at mammalian carotid body chemoreceptors. *Semin Cell Dev Biol* **24**, 22–30.

Ortega F, Pérez-Sen R & Miras-Portugal MT (2008). Gi-coupled P2Y-ADP receptor mediates GSK-3 phosphorylation and β-catenin nuclear translocation in granule neurons. *J Neurochem* **104**, 62–73.

Pace RW, Mackay DD, Feldman JL & Del Negro CA (2007). Inspiratory bursts in the preBötzinger complex depend on a calcium-activated non-specific cation current linked to glutamate receptors in neonatal mice. *J Physiol* **582**, 113–125.

Parkis MA, Dong X, Feldman JL & Funk GD (1999). Concurrent inhibition and excitation of phrenic motoneurons during inspiration: phase-specific control of excitability. *J Neurosci* **19**, 2368–2380.

Partridge LD, Müller TH & Swandulla D (1994). Calcium-activated non-selective channels in the nervous system. *Brain Res Brain Res Rev* **19**, 319–325.

Perrier JF & Hounsgaard J (1999). Ca^{2+}-activated nonselective cationic current (I_{CAN}) in turtle motoneurons. *J Neurophysiol* **82**, 730–735.

Perrier JF, Mejia-Gervacio S & Hounsgaard J (2000). Facilitation of plateau potentials in turtle motoneurones by a pathway dependent on calcium and calmodulin. *J Physiol* **528**, 107–113.

Poelchen W, Sieler D, Wirkner K & Illes P (2001). Co-transmitter function of ATP in central catecholaminergic neurons of the rat. *Neuroscience* **102**, 593–602.

Powers RK & Binder MD (2003). Persistent sodium and calcium currents in rat hypoglossal motoneurons. *J Neurophysiol* **89**, 615–624.

Price GD, Robertson SJ & Edwards FA (2003). Long-term potentiation of glutamatergic synaptic transmission induced by activation of presynaptic P2Y receptors in the rat medial habenula nucleus. *Eur J Neurosci* **17**, 844–850.

Rae MG, Rowan EG & Kennedy C (1998). Pharmacological properties of $P2X_3$-receptors present in neurones of the rat dorsal root ganglia. *Br J Pharmacol* **124**, 176–180.

Ravi RG, Kim HS, Servos J, Zimmermann H, Lee K, Maddileti S, Boyer JL, Harden TK & Jacobson KA (2002). Adenine nucleotide analogues locked in a Northern methanocarba conformation: enhanced stability and potency as $P2Y_1$ receptor agonists. *J Med Chem* **45**, 2090–2100.

Rekling JC & Feldman JL (1997). Calcium-dependent plateau potentials in rostral ambiguus neurons in the newborn mouse brain stem in vitro. *J Neurophysiol* **78**, 2483–2492.

Richardson PJ & Brown SJ (1987). ATP release from affinity-purified rat cholinergic nerve terminals. *J Neurochem* **48**, 622–630.

Robson SC, Sevigny J & Zimmermann H (2006). The E-NTPDase family of ectonucleotidases: Structure function relationships and pathophysiological significance. *Purinergic Signal* **2**, 409–430.

Ruangkittisakul A, Schwarzacher SW, Secchia L, Poon BY, Ma Y, Funk GD & Ballanyi K (2006). High sensitivity to neuromodulator-activated signaling pathways at physiological $[K^+]$ of confocally imaged respiratory center neurons in on-line-calibrated newborn rat brainstem slices. *J Neurosci* **26**, 11870–11880.

Sak K & Illes P (2005). Neuronal and glial cell lines as model systems for studying P2Y receptor pharmacology. *Neurochem Int* **47**, 401–412.

Schwindt P & Crill WE (1977). A persistent negative resistance in cat lumbar motoneurons. *Brain Res* **120**, 173–178.

Shimamura K, Zhou M, Ito Y, Kimura S, Zou LB, Sekiguchi F, Kitramura K & Sunano S (2002). Effects of flufenamic acid on smooth muscle of the carotid artery isolated from spontaneously hypertensive rats. *J Smooth Muscle Res* **38**, 39–50.

Simon J, Webb TE, King BF, Burnstock G & Barnard EA (1995). Characterisation of a recombinant P2Y purinoceptor. *Eur J Pharmacol* **291**, 281–289.

Smith JC, Ellenberger HH, Ballanyi K, Richter DW & Feldman JL (1991). Pre-Bötzinger complex: a brainstem region that may generate respiratory rhythm in mammals. *Science* **254**, 726–729.

Smith JC & Feldman JL (1987). In vitro brainstem-spinal cord preparations for study of motor systems for mammalian respiration and locomotion. *J Neurosci Methods* **21**, 321–333.

Sobrinho CR, Wenker IC, Poss EM, Takakura AC, Moreira TS & Mulkey DK (2014). Purinergic signalling contributes to chemoreception in the retrotrapezoid nucleus but not the nucleus of the solitary tract or medullary raphe. *J Physiol* **592**, 1309–1323.

Spruston N, Jaffe DB, Williams SH & Johnston D (1993). Voltage- and space-clamp errors associated with the measurement of electrotonically remote synaptic events. *J Neurophysiol* **70**, 781–802.

Stuart GJ, Dodt HU & Sakmann B (1993). Patch-clamp recordings from the soma and dendrites of neurons in brain slices using infrared video microscopy. *Pflugers Arch* **423**, 511–518.

Suzue T (1984). Respiratory rhythm generation in the *in vitro* brain stem–spinal cord preparation of the neonatal rat. *J Physiol* **354**, 173–183.

Thomas T, Ralevic V, Bardini M, Burnstock G & Spyer KM (2001). Evidence for the involvement of purinergic signalling in the control of respiration. *Neuroscience* **107**, 481–490.

Ullrich ND, Voets T, Prenen J, Vennekens R, Talavera K, Droogmans G & Nilius B (2005). Comparison of functional properties of the Ca^{2+}-activated cation channels TRPM4 and TRPM5 from mice. *Cell Calcium* **37**, 267–278.

van Brederode JF, Yanagawa Y & Berger AJ (2011). GAD67-GFP+ neurons in the Nucleus of Roller: a possible source of inhibitory input to hypoglossal motoneurons. I. Morphology and firing properties. *J Neurophysiol* **105**, 235–248.

Viana F, Gibbs L & Berger AJ (1990). Double- and triple-labeling of functionally characterized central neurons projecting to peripheral targets studied *in vitro*. *Neuroscience* **38**, 829–841.

von Kugelgen I (2006). Pharmacological profiles of cloned mammalian P2Y-receptor subtypes. *Pharmacol Ther* **110**, 415–432.

von Kugelgen I & Wetter A (2000). Molecular pharmacology of P2Y-receptors. *Naunyn Schmiedebergs Arch Pharmacol* **362**, 310–323.

Yao ST, Barden JA & Lawrence AJ (2001). On the immunohistochemical distribution of ionotropic P2X receptors in the nucleus tractus solitarius of the rat. *Neuroscience* **108**, 673–685.

Yasuda K, Robinson DM, Selvaratnam SR, Walsh CW, McMorland AJ & Funk GD (2001). Modulation of hypoglossal motoneuron excitability by NK1 receptor activation in neonatal mice *in vitro*. *J Physiol* **534**, 447–464.

Zhang B, Wootton JF & Harris-Warrick RM (1995). Calcium-dependent plateau potentials in a crab stomatogastric ganglion motor neuron. II. Calcium-activated slow inward current. *J Neurophysiol* **74**, 1938–1946.

Zwicker JD, Rajani V, Hahn LB & Funk GD (2011). Purinergic modulation of preBötzinger complex inspiratory rhythm in rodents: the interaction between ATP and adenosine. *J Physiol* **589**, 4583–4600.

Additional information

Competing interests

The authors have no competing interests to declare.

Author contributions

T.S.A. performed all experiments and data analysis procedures associated with analysis of effects of GABA and P2YR agents on C4 and XII burst amplitude, and whole-cell recording experiments that assessed the effects of P2YR agents on the synaptic and membrane properties of XII MNs, excluding those involved in analysing the PIC. He also contributed to experimental design, article drafting, figure production and revision, and final approval. A.L.R. performed all experiments and data analysis procedures associated with analysis of the PIC in XII MNs. She also contributed to experimental design of this component of the study, article drafting, figure production and revision, and final approval. A.G.H. performed the immunohistochemical analysis of $P2Y_1R$, NK1R and ChAT and expression in XII MNs, as well as the preparation of related figures, and final approval. C.D.L. performed the laser-capture microdissection of XII MNs and real-time PCR analysis of TRPM4 and TRPM5 transcript expression, and final approval. G.D.F. oversaw all aspects of the study, from conception to final publication. All experiments were performed in the laboratory of G.D.F., Dept Physiol, University of Alberta. All authors approved the final version of the manuscript.

Funding

This work was supported by the Canadian Institutes of Health Research (CIHR 53085, RES0006842), the Natural Sciences and Engineering Research Council of Canada (NSERC 402532, RES0012299), Alberta Innovates–Health Solutions (AIHS), the Women and Children's Health Research Institute (Alberta, Canada), the Canada Foundation for Innovation, and the Alberta Science and Research Authority. G.D.F. is an AIHS Scientist.

Acknowledgements

None declared.